Graphical Abstract

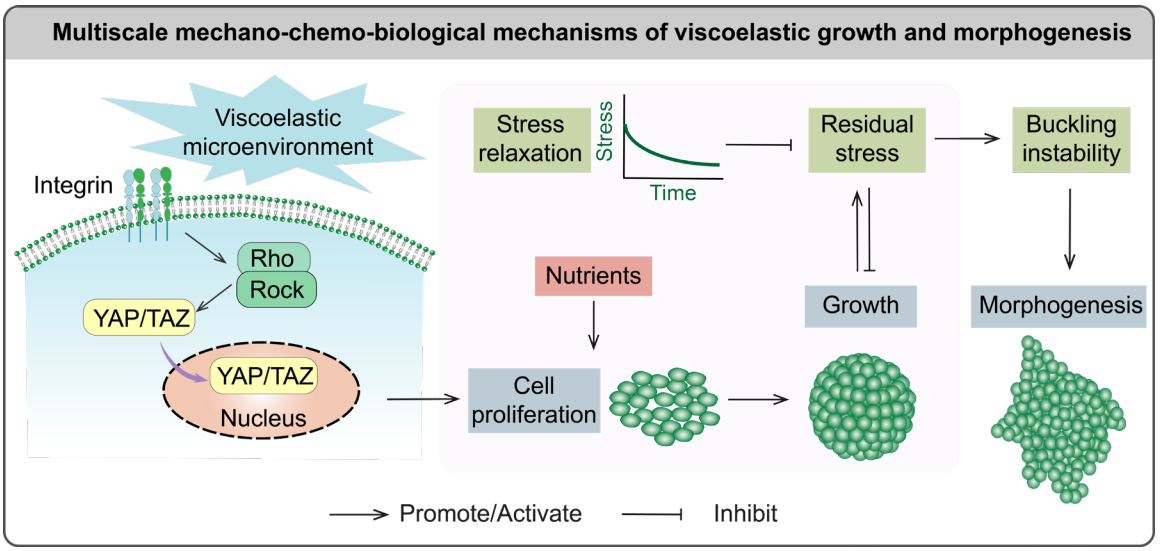

A multiscale mechano-chemo-biological model is proposed to reveal the influences of viscoelasticity on the growth and morphogenesis of soft biological tissues and organs.

Highlights

- A multiscale mechano-chemo-biological model is proposed for the growth and morphogenesis of soft tissues.
- Viscoelasticity significantly modulates the stress accumulation and growth of soft tissues and organs.
- Viscoelastic effects on the surface instability and morphogenesis of growing organoids are revealed.

Mechanobiological modeling of viscoelasticity in soft tissue growth and morphogenesis

Zhongya Lin[1], Weizhi Huang[1], Shuang Li[1], Mingfeng Wang[2], Jinshuai Bai[1], Xindong Chen[1], Xi-Qiao Feng[1,3,*]

[1] *Institute of Biomechanics and Medical Engineering, AML Department of Engineering Mechanics, Tsinghua University, Beijing 100084, China*

[2] *Institute of Applied Mechanics, University of Stuttgart, Pfaffenwaldring 7, Stuttgart, Germany*

[3] *Mechano-X Institute, Tsinghua University, Beijing 100084, China*

Abstract

Most soft biological tissues feature distinct mechanical properties of viscoelasticity, which play a significant role in their growth, development, and morphogenesis. In this paper, we propose a mechanobiological viscoelastic model in the framework of thermodynamics. The multiscale mechanisms underlying the viscoelasticity of tissues are clarified, such as extracellular matrix composition and organization, cell types and states, dynamic cell–matrix and cell–cell interactions, and active cytoskeleton evolution. This model enables us to elucidate how viscoelastic effects modulate the growth and surface instability of soft tissues via coupled mechano-chemo-biological regulatory mechanisms. The proposed constitutive model is implemented into the finite element method, to explore the growth, stability, and morphological evolution of tissues. Illustrative examples, including tumor growth and organoid development, demonstrate that viscoelasticity can facilitate sustained tissue growth, and significantly influences the critical conditions of surface wrinkling and the morphological evolution of tissues. The results are consistent with relevant experimental observations. This study provides a theoretical model for growing soft tissues with viscoelastic effects, and holds promise for potential applications in clinical diagnosis and treatment of some diseases.

Keywords: Soft tissue; Growth; Viscoelasticity; Mechano-chemo-biological mechanism; Instability; Morphological evolution.

* Corresponding author: fengxq@tsinghua.edu.cn (X.-Q. Feng)

1. Introduction

Biological tissues coordinate a complex array of functions crucial for physiological processes and structural integrity, which depend on the complicated yet precisely designed interplay between biochemical compositions and mechanical properties (Cambria et al., 2024; McGinn et al., 2021). During growth and development, tissues exhibit both recoverable elastic deformation and time-dependent viscous behavior, known as viscoelasticity. Their mechanical properties may vary in response to external stimuli, biochemical signals, and pathological conditions (Katira et al., 2013; Persson et al., 2020). In recent years, the effects of viscoelastic properties on tissue development and pathology have gathered extensive attention (Clément et al., 2017; Fan et al., 2024).

Viscoelasticity is an intrinsic mechanical property of biological tissues (Fig. 1), e.g., brain, skin, cartilage, blood vessels, and solid tumors (Hadzipasic et al., 2023; Zhang et al., 2021). The viscoelastic properties of soft tissues originate from the combination of multiscale mechano-chemo-biological mechanisms, including active cytoskeleton evolution, cell density, cell division and arrangements, extracellular matrix compositions, and the duration of external forces (Huang et al., 2019). Due to the specificity and complexity of these mechanisms, the viscoelastic properties of different tissues exhibit a distinct diversity. For illustration, the different stress relaxation rates of a few representative soft tissues are shown in Fig. 1a. Viscoelasticity plays a crucial role in volumetric growth, morphological development, biological functions, and responses to various mechanical and biochemical cues (Mierke, 2022). During embryonic development, for example, the posterior tissues undergo viscoelastic changes from a fluid-like state to a solid-like one, which allows for the elongation of the vertebrate body axis (Mongera et al., 2018). The viscoelastic properties of the matrix can influence the proliferation and differentiation of stem cells by regulating integrin-based adhesion, actomyosin contractility, and nuclear localization of Yes-associated protein (YAP) (Chaudhuri et al., 2016). In wound healing, the fluidization of tissue, corresponding to a reduction in cell junctional tension and cell–cell adhesion, allows for faster wound closure through increased cell movement and rearrangement (Tetley et al., 2019). Appropriate viscoelastic properties may also enhance tissue regeneration by promoting favorable cellular activities (Patiño Vargas et al., 2022), which may reduce scar thickness and ensure the restoration of tissue function. Pathological changes, such as cancer progression, fibrosis, and tissue degeneration are also closely related to viscoelasticity. Tumor cells can sense tissue stiffness and viscoelasticity, which may affect their biochemical signaling pathways and

proliferation (Fan et al., 2024). Furthermore, viscosity may affect the epigenetics of cancer cells to form mechanical memory (Li et al., 2024), which impacts the development of cancer (Bera et al., 2022). Fibrosis is associated with alterations in viscoelastic properties. Monitoring viscoelasticity changes may aid in the early diagnosis of fibrosis before significant tissue stiffening occurs (Long et al., 2021; Reiter et al., 2021). Brain episodic memory performance is related to hippocampal viscoelasticity, and it can serve as a biomarker corresponding to cognitive decline due to aging or brain diseases (Hiscox et al., 2021). In the field of tissue engineering, viscoelastic properties are critical for designing scaffolds that can mimic the mechanical behavior of native tissues (Foroughi et al., 2023). Therefore, it is significant to elucidate the mechanical, chemical, and biological mechanisms underlying the viscoelastic effects of tissues, which affect their deformation, development, adaptation, and structural integrity under different physiological and pathological conditions. Recent studies also suggest that understanding viscoelastic effects may help develop novel diagnostic and therapeutic strategies (Chang et al., 2023; Wu et al., 2022).

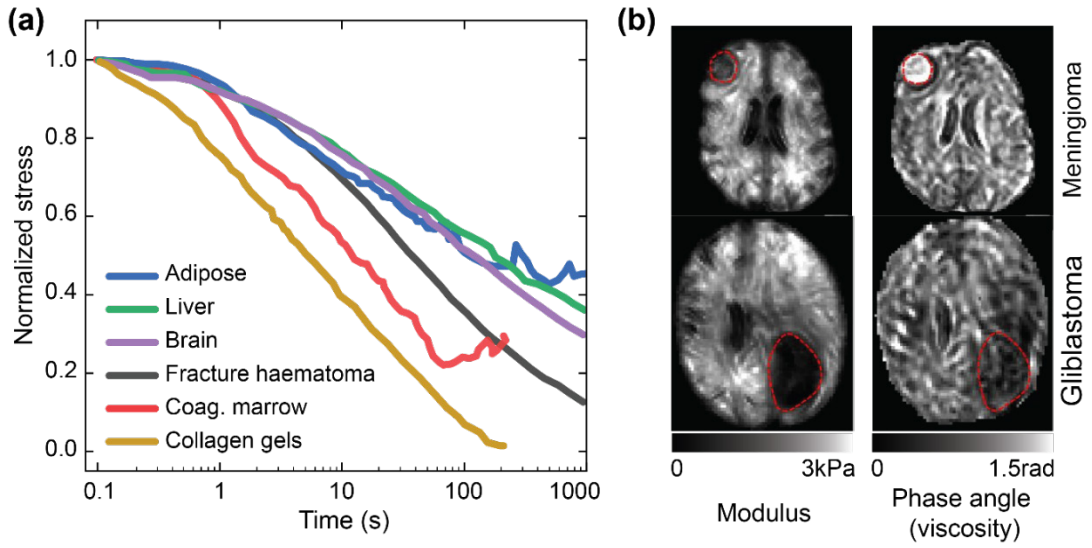

Fig. 1. Viscoelasticity of soft biological tissues. (a) Stress relaxation curves of tissues and collagen gels, which demonstrate significant viscoelastic properties, adapted from (Chaudhuri et al., 2020). (b) Viscoelasticity of two brain tumors, with different moduli and phase angles of viscosity; adapted from (Streitberger et al., 2020). The two tumors have different growth rates and invasion capabilities.

Much experimental effort has been directed toward exploring the viscoelastic properties effects and mechanisms of tissues. Such experimental techniques as rheometer, atomic force microscopy (AFM), and magnetic resonance elastography (MRE) have been employed to quantify the viscoelastic properties of various tissues (Huang et al., 2019; Zhang et al., 2021).

The rheometer determines the viscoelastic properties by applying oscillatory shear stresses to a tissue and measuring the resultant strains under different loading conditions (Hobson et al., 2021). AFM offers high-resolution mapping of static or dynamic mechanical properties at the cellular and subcellular levels, enabling the study of local variations within tissues (Rebelo et al., 2013; Rother et al., 2014). MRE provides a non-invasive method to assess the mechanical properties of tissues *in vitro* and *in vivo*. This capability allows for monitoring changes in viscoelastic properties induced by disease progression or treatment, such as liver fibrosis, brain tumors, and cardiovascular diseases (Reiter et al., 2021; Zhang et al., 2021). These investigations are valuable for understanding the mechanical behavior of tissues under different physiological and pathological conditions. Studies using these techniques have revealed that viscoelasticity can regulate spatiotemporal tissue organization, driving tissue growth dynamics and symmetry-breaking instabilities like buckling, folding, and fingering (Mao and Wickström, 2024). *In vitro* experiments have shown that tumors grow more rapidly in the viscoelastic environment compared to their elastic counterpart, with viscoelasticity leading to early branching or morphological instability (Elosegui-Artola et al., 2022). Different types of brain tumors exhibit significantly different viscoelastic properties (Fig. 1b), leading to their different growth rates and invasive behaviors. Consequently, targeting the viscoelastic properties of the tumor microenvironment could be a novel approach to inhibit tumor growth and metastasis (Streitberger et al., 2020). These experimental findings provide a foundation for theoretical modeling to capture the complex interplay among viscoelasticity, tissue growth, and morphological evolution.

The biomechanical mass stress relation proposed in the 1990s (Fung, 1990) states that growth and remodeling mechanics should account for the changes in the stress-free configuration due to mass changes. It provides a framework for modeling the growth and remodeling of living tissues. On this basis, quite a few hyperelastic theoretical models have been developed to describe the growth of tissues. Usually, these models introduce a set of kinematic and kinetic equations to capture the complex interactions between mechanical forces and biological processes (Goriely, 2017; Sun et al., 2022). The hyperelastic continuum model provides a valuable framework for understanding the elastic behavior of tissues and their responses to mechanical forces. Residual stresses, arising from differential and incompatible growth and deformation, play a pivotal role in the growth and various morphogenetic processes, such as tissue folding and branching (Ambrosi et al., 2019; Xu et al., 2022). The porous matrix biomechanical model, which treats the tissue as a composite material consisting of a solid

matrix and a fluid-filled pore space, has also been employed to study growth-induced solid stresses within tissues (Xue et al., 2018; Xue et al., 2016). The coupling effects between the solid and fluid phases are important for the growth and morphological evolution of tissues under different physiological and pathological conditions. The incremental hyperelastic constitutive method, incorporating constraint conditions such as incompressibility and interfacial continuity, has been used in the analysis of growth-induced instabilities (Ben Amar and Goriely, 2005; Huang et al., 2024; Wang et al., 2023). It characterizes how tissues respond to incremental changes in volumetric growth and mechanical loading, providing a more nuanced understanding of the conditions that lead to instability and subsequent development of complex tissue patterns. These previous significant works mainly concentrate on the elastic components or mechanical interactions, and they have not examined the time-dependent viscoelastic behaviors of tissues. Recently, a finite hyper-viscoelastic model has been developed to capture the nonlinear viscous effects of soft tissues under complex loading (Panda and Buist, 2018). The Prony-series viscoelastic model is employed to capture the complex viscoelastic behaviors of different brain regions (Morrison et al., 2023). The Saffman-Taylor instability model has been applied to explain why brain tumors with higher viscosity are more aggressive and infiltrative (Streitberger et al., 2020). The buckling instability of epithelial tissues is a key issue in developmental biology. A multiscale biomechanical study elucidated that viscoelasticity contributes significantly to both the buckling mode and the postbuckling phase transition of an epithelial monolayer (Wang et al., 2024). These viscoelastic models help understand how tissues gradually respond to mechanical stimuli over time and the long-term viscoelastic behavior of tissues. However, viscoelastic models should be combined with growth laws to fully capture the interplay between time-dependent mechanical stimuli, tissue growth, and buckling instability processes.

In this paper, by considering the mechano-chemo-biological mechanisms involved in the development of soft tissues, we present a mechanobiological viscoelastic model to investigate the viscoelastic effects on their growth, instability, and morphological evolution. This paper is organized as follows. In Section 2, we present the mechano-chemo-biological mechanisms of tissue viscoelasticity, and then formulate a mechanobiological growth model with viscoelastic and nutrition concertation effects. In Section 3, through the spherical shell–core model for a tumor spheroid, we examine the impact of viscoelasticity on the residual stress accumulation and growth rate. Section 4 analyzes the influences of viscoelasticity on the instability and morphological evolution of the spherical organoid with differential growth. This is

accomplished through the finite element method by implementing the proposed constitutive model. Finally, the main conclusions drawn from this study are summarized in Section 5.

2. Mechanobiological model

2.1. Mechano-chemo-biological mechanisms of tissue viscoelasticity

Both elastic and viscous properties are significant for soft tissues to withstand and adapt to their dynamic biomechanical environments. The viscoelasticity of tissues has been studied in many experiments (Fig. 2a), which results from complicated mechano-chemo-biological mechanisms (Fig. 2b). Viscoelasticity can change with growth and development under pathological and physiological conditions (Cox, 2021; Huang et al., 2019). For instance, a compact arrangement of cells exhibits more solid-like properties, whereas a dispersed arrangement displays more fluid-like behavior (Mao and Wickström, 2024). The fluid-to-solid transformation may play an important role in embryonic development (Mongera et al., 2018). Due to cell differentiation, proliferation, and carcinogenesis, tissues may contain various types of cells with different structural and mechanical properties in order to achieve their biological functions (Hang et al., 2022). The extracellular matrix (ECM) provides mechanical, chemical, and structural support to tissues. The density and orientation of ECM fibrils, such as collagen and elastin, play a significant role in the variation of tissue viscoelastic properties (Chaudhuri et al., 2020; Lyu et al., 2023). In addition, the interactions of cell–ECM and cell–cell, mediated by integrins, cadherins and other adhesion molecules, are vital for maintaining the integrity and distributing the mechanical stresses in the tissue. (Mao and Wickström, 2024). At the subcellular scale, the evolution of the cytoskeleton (Pegoraro et al., 2017) and cell cortex (Yin et al., 2022) may significantly influence the viscoelastic properties of cells and thereby determine how tissues respond to external stimuli. Therefore, the types and arrangements of cells within the tissue, ECM properties, cell interactions and actin cytoskeleton evolution collectively determine the macroscale viscoelastic property of a tissue (Fig. 2b). In Appendix B, we try to clarify how these multiscale mechanisms modulate the viscoelastic parameters.

To accurately characterize the viscoelastic behavior of soft tissues, it is crucial to utilize a theoretical model that can encapsulate these multifaceted interactions. Some simple viscoelastic models consisting of springs and dashpots have been used to describe the viscoelastic properties of tissues (Elosegui-Artola et al., 2022; Mongera et al., 2023). In this study, the specific viscoelastic properties are tentatively modeled by a three-parameter

viscoelastic model (Fig. 2c), which is a combination of spring and dashpot elements (Lin and Wei, 2020). This model serves as a bridge, linking the mechano-chemo-biological properties at the cellular and molecular levels to the observable macroscopic viscoelastic behavior of the tissue. The variations in the relaxation modulus and relaxation time are correlated with these multiscale mechanisms and their changes. These variations further affect the values of the viscoelastic moduli, which can be formulated, for example, as $G(t) = G_\infty + G_1 \exp(-t\, G_1 / \xi)$. This function will be employed to distinguish the specific types of tissues and to characterize the temporal evolution of their viscoelastic behavior. Furthermore, this viscoelastic model will be integrated into the tissue growth law in the following section.

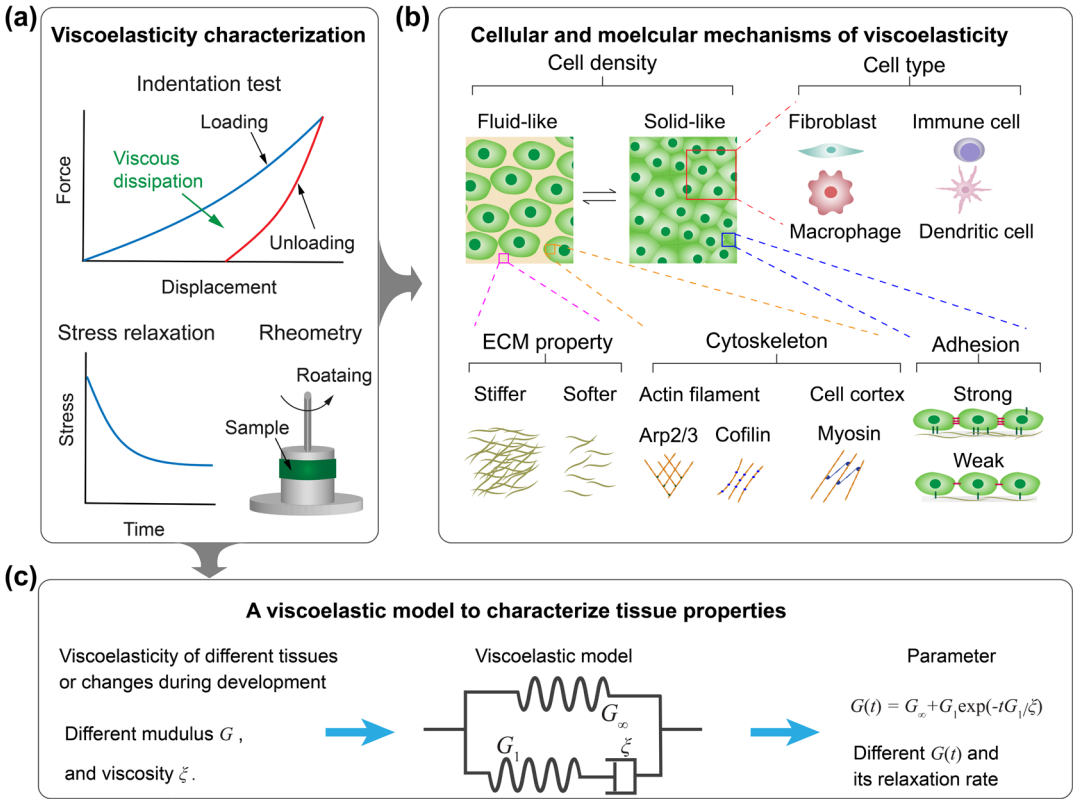

Fig. 2. Mechanisms and modeling of viscoelastic properties of soft tissues. (a) Viscoelastic behavior of tissues tested by many experimental techniques. (b) Cellular and molecular mechanisms underlying the elastic and viscoelastic behaviors of a tissue. (c) A three-parameter viscoelastic model is here taken as an example to characterize the viscoelasticity of different tissues and changes in viscoelasticity, through the different viscoelastic moduli and relaxation times.

2.2. Mechanobiological growth model with viscoelastic effects

Consider a body in the three-dimensional Euclidean space $\mathbb{E}3$, as shown in Fig. 3, where Ω_0 is the initial (reference) configuration (at time t_0), and Ω is the current configuration (at time t). $\boldsymbol{X}$ and $\boldsymbol{x}$ denote the positions of a material point in the two configurations, respectively.

For a tissue with differential volume growth and large deformation, we adopt the decomposition of the deformation gradient tensor $\mathbf{F}$ (Rodriguez et al., 1994; Zhou et al., 2018). It is expressed as

$$\mathbf{F} = \mathbf{F}_a \cdot \mathbf{F}_g \,, \tag{1}$$

where $\mathbf{F}_a$ denotes the mechanical deformation tensor with the viscoelastic effect, and $\mathbf{F}_g$ denotes the growth tensor. A stress-free intermediate configuration Ω_v is also defined, which is often incompatible in the case of differential growth, as illustrated in Fig. 3. Due to the viscoelastic effect, i.e., stress relaxation and creep, the deformation tensor evolves, leading to the evolution of both the intermediate and current configurations. The synergistic effects of elastic and viscoelastic deformation and volumetric growth may greatly influence the morphological instability and evolutions of tissues under various physiological and pathological conditions, as we will show below.

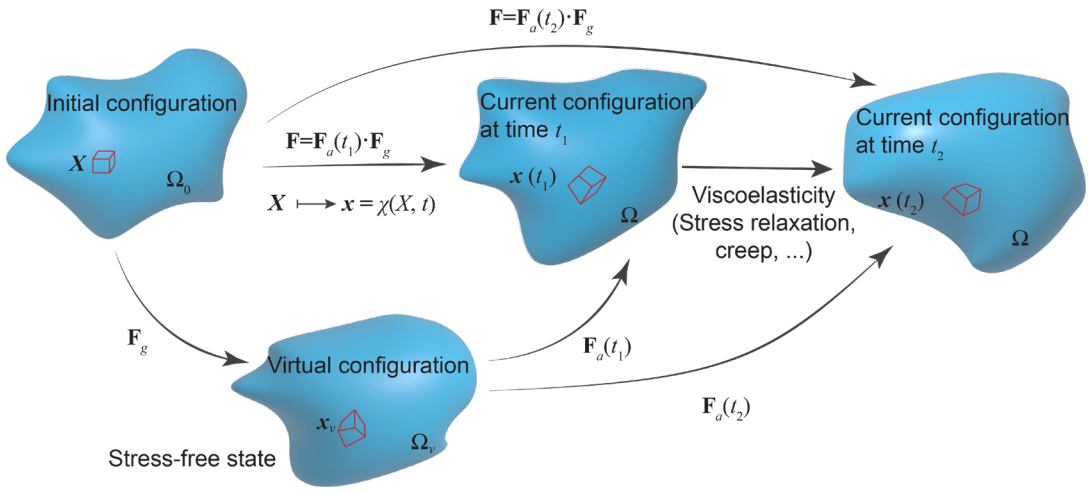

Fig. 3. Schematic diagram of multiplicative decomposition. The growth tensor $\mathbf{F}_g$ at time t_1 leads to the current configuration $\Omega(t_1)$, and the corresponding deformation gradient is decomposed into $\mathbf{F}_a(t_1)$ and $\mathbf{F}_g$. The situation is similar for at time t_2. A material point with the coordinate vector $\boldsymbol{X}$ in the initial configuration is mapped to $\boldsymbol{x}$ in the current configuration by $\chi(\boldsymbol{X}, t)$. The viscoelasticity leads to time-dependent deformation, which evolves with time.

2.2.1. Mass balance equation

In general, tissue growth can occur through coupled volumetric growth and material flux across its boundary $\partial\Omega$. Let the volumetric growth function $\rho\gamma_g$ denote the mass increase due to cell proliferation or ECM synthesis per unit volume in the current configuration, where $\gamma_g(\boldsymbol{x})$ is the growth rate function and ρ=dm/dV is the mass density. The flux of material through the boundary corresponds to the vector $\mathbf{R}_f$. Thus, the mass balance is

$$\frac{\mathrm{d}}{\mathrm{d}t}\int_{\Omega}(\mathrm{d}m)=\frac{\mathrm{d}}{\mathrm{d}t}\int_{\Omega}(\rho\mathrm{d}V)=\int_{\Omega}\rho\gamma_g\mathrm{d}V+\int_{\partial\Omega}\mathbf{R}_f\cdot\mathbf{n}\mathrm{d}S\,. \tag{2}$$

The volume rate is proportional to the divergence of the velocity field, that is,

$$\frac{\mathrm{d}}{\mathrm{d}t}(\mathrm{d}V)=\mathrm{div}\,\mathbf{v}\,\mathrm{d}V, \tag{3}$$

where $\mathbf{v}$ denotes the velocity vector. By applying the divergence theorem, the mass balance equation for a growing continuum can be obtained from Eq. (2) as

$$\dot{\rho}+\rho\,\mathrm{div}\,\mathbf{v}=\rho\gamma_g+\mathrm{div}\mathbf{R}_f, \tag{4}$$

where the dot above the variable stands for the material time derivative. In the case of slow growth, the flux through the boundary can be neglected (Ben Amar and Goriely, 2005; Goriely, 2017), we have

$$\dot{\rho}+\rho\,\mathrm{div}\,\mathbf{v}=\rho\gamma_g. \tag{5}$$

Let ρ_0 and ρ_g denote the densities in the initial state and the virtual stress-free state, respectively. The mass growth can also be written as

$$\frac{\mathrm{d}}{\mathrm{d}t}\int_{\Omega}(\rho_g\mathrm{d}V_g)=\int_{\Omega}\rho_g\gamma_g\mathrm{d}V_g\,, \tag{6}$$

where $\rho_g=\mathrm{d}m_g/\mathrm{d}V_g=\mathrm{d}m/\mathrm{d}V_g$, $J_g=\det(\mathbf{F}_g)$, $\mathrm{d}V_g=J_g\mathrm{d}V_0$ and $J=J_aJ_g=\det(\mathbf{F}_a)\det(\mathbf{F}_g)$ are the measurement of the volume change. $\mathrm{d}V_0$ denotes the initial volume element. When the same mass density is assumed for the new tissue generated by growth and the original one, that is, the constant density growth $\rho_0=\rho_g$, we obtain

$$\gamma_g=J_g^{-1}\dot{J}_g=\mathrm{tr}(\mathbf{F}_g^{-1}\cdot\dot{\mathbf{F}}_g), \tag{7}$$

where $\dot{J}_g=J_g\mathrm{tr}(\mathbf{F}_g^{-1}\cdot\dot{\mathbf{F}}_g)$ is the Jacobi's formula.

2.2.2. Momentum balance equation

We assume that the newly added material due to tissue growth has the same properties as the original one. Thus, the linear momentum balance of the growing tissue can be expressed as

$$\frac{\mathrm{d}}{\mathrm{d}t}\int_{\Omega}\rho\mathbf{v}\mathrm{d}V=\int_{\partial\Omega}\mathbf{t}\mathrm{d}S+\int_{\Omega}\rho\mathbf{f}\mathrm{d}V+\int_{\Omega}\rho\gamma_g\mathbf{v}\mathrm{d}V\,, \tag{8}$$

where $\mathbf{t}$ and $\mathbf{f}$ denote the surface traction and the body force, respectively. The surface traction vector is related to the Cauchy stress, $\mathbf{t}=\sigma\cdot\mathbf{n}$, where $\mathbf{n}$ is the unit outward normal to the

surface. Using the divergence theorem and Eq. (5), the differential form of Eq. (8) gives, that is, the balance of linear momentum (Rahman et al., 2017)

$$\rho\dot{\mathbf{v}} = \mathrm{div}(\sigma^{\mathrm{T}}) + \rho\mathbf{f}. \tag{9}$$

Furthermore, the acceleration can be ignored for slow growth. In the absence of the body force, then Eq. (9) becomes

$$\mathrm{div}(\sigma) = 0. \tag{10}$$

The balance between the angular momentum and the applied torques for a growing continuum can be expressed as

$$\frac{\mathrm{d}}{\mathrm{d}t}\int_{\Omega}\rho\mathbf{x}\times\mathbf{v}\mathrm{d}V = \int_{\partial\Omega}\mathbf{x}\times\mathbf{t}\mathrm{d}S + \int_{\Omega}\rho\mathbf{x}\times\mathbf{f}\mathrm{d}V + \int_{\Omega}\rho\gamma_g\mathbf{x}\times\mathbf{v}\mathrm{d}V\,. \tag{11}$$

The transport and localization procedure lead to the symmetric condition for the Cauchy stress tensor $\sigma = \sigma^{\mathrm{T}}$.

2.2.3. Energy and entropy equation

The kinetic energy equation for an isothermal growth at a physiological temperature can be expressed as (Ciarletta et al., 2012)

$$\frac{\mathrm{d}}{\mathrm{d}t}\int_{\Omega}K\mathrm{d}V = P_i + P_e, \tag{12}$$

where K is the kinetic energy per unit volume, P_i and P_e denote the internal and external rates of mechanical work, respectively. Thus, they read

$$P_i = -\int_{\Omega}\sigma\colon\mathbf{D}\mathrm{d}V\,, \tag{13}$$

$$P_e = -\int_{\Omega}\rho\mathbf{f}\cdot\mathbf{v}\mathrm{d}V + \int_{\partial\Omega}\mathbf{t}\cdot\mathbf{v}\mathrm{d}S + \frac{1}{2}\int_{\Omega}\rho\gamma_g\mathbf{v}\cdot\mathbf{v}\mathrm{d}V\,, \tag{14}$$

where $\mathbf{D} = 1/2\left[\dot{\mathbf{F}}\cdot\mathbf{F}^{-1} + \left(\dot{\mathbf{F}}\cdot\mathbf{F}^{-1}\right)^{\mathrm{T}}\right]$ is the deformation rate.

Then, the first law of thermodynamics is applied to a growing continuum as the conversation of energy principle, that is,

$$\frac{\mathrm{d}}{\mathrm{d}t}\int_{\Omega}(\rho e + K)\mathrm{d}V = P_e + \int_{\Omega}\rho\gamma_g e\mathrm{d}V + \int_{\Omega}\mathbf{b}_g\colon\mathbf{L}_g\mathrm{d}V + Q, \tag{15}$$

where e is the internal energy per unit current mass, $\mathbf{L}_g = \dot{\mathbf{F}}_g \cdot \mathbf{F}_g^{-1}$ denotes the growth rate tensor. $\mathbf{b}_g$ denotes the homeostatic stress, which represents the biochemical and cellular activity involved in the growth process (Buskohl et al., 2014), and it work-conjugate to the growth rate tensor (DiCarlo and Quiligotti, 2002). Q represents the total heat input rate, which is given as

$$Q = \int_\Omega \rho\omega \mathrm{d}V - \int_{\partial\Omega} \mathbf{q} \cdot \mathbf{n} \mathrm{d}S\,, \tag{16}$$

where ω is the heat input rate per unit current mass, $\mathbf{q}$ is the heat flux across the surface element. Therefore, the energy balance equation reads

$$\rho\dot{e} = \sigma : \mathbf{D} + \mathbf{b}_g : \mathbf{L}_g + \rho\omega - \mathrm{div}(\mathbf{q}). \tag{17}$$

Entropy measures the disorder induced by microscopic fluctuations. For a growing continuum, the integral form of the entropy equation can be expressed as

$$\frac{\mathrm{d}}{\mathrm{d}t}\int_\Omega \rho s \mathrm{d}V = \int_\Omega \rho\gamma_g s \mathrm{d}V + \int_\Omega \rho\eta \mathrm{d}V + + \int_\Omega \frac{\rho\omega}{T}\mathrm{d}V - \int_{\partial\Omega} \frac{1}{T}\mathbf{q} \cdot \mathbf{n} \mathrm{d}S\,, \tag{18}$$

where s and η denote the entropy and the entropy production rate per unit current mass, respectively, T is the absolute temperature. Applying the divergence theorem and the transport equation Eq. (S5), it has

$$\rho\dot{s} = \frac{\rho\omega}{T} - \mathrm{div}\frac{\mathbf{q}}{T} + \rho\eta. \tag{19}$$

The second law of thermodynamics states that the internal entropy change rate of a system should not be smaller than the flow of entropy transferred to that system, that is $\eta \geq 0$. Therefore, from Eq. (19), the Clausius–Duhem inequality requires that

$$\rho\dot{s} \geq \frac{\rho\omega}{T} - \mathrm{div}\frac{\mathbf{q}}{T}. \tag{20}$$

The relation between the specific internal energy e and the specific free energy ψ can be obtained from the Legendre transformation,

$$\psi = e - Ts. \tag{21}$$

Combining Eqs. (17), (20) and (21), we obtain the inequality

$$\rho\dot{\psi} \leq \sigma : \mathbf{D} + \mathbf{b}_g : \mathbf{L}_g - \rho s\dot{T} - \frac{1}{T}\mathbf{q} \cdot \mathrm{grad}(T). \tag{22}$$

314 *2.2.4. Viscoelastic constitutive relation of growing tissues*

315 Assume that the deformation gradient $F_{ij}(t)$ and temperature $T(t)$ are continuous in the
316 interval $0 < t < \infty$, that is, it follows from the Stone-Weierstrass theorem. Referring to the
317 polynomial expansion of the free energy in terms of Stieltjes integrals (Christensen and Naghdi,
318 1967), $\rho\psi$ can be simplified as

319
$$\rho\psi = \rho\psi_0 + \int_{-\infty}^{t} \mathbf{A}(t-\zeta) : \frac{\partial \mathbf{F}_a}{\partial \zeta} \mathrm{d}\zeta - \int_{-\infty}^{t} \beta(t-\zeta) \frac{\partial T_d}{\partial \zeta} \mathrm{d}\zeta + W_c(\mathbf{F}_a, t) - \int_{-\infty}^{t}\int_{-\infty}^{t} \kappa(t-\zeta_1, t-\zeta_2) \frac{\partial T_d}{\partial \zeta_1} \frac{\partial T_d}{\partial \zeta_2} \mathrm{d}\zeta_1 \, \mathrm{d}\zeta_2 + \cdots, \quad (23)$$

320 where ψ_0 is the mean free energy, $T_d(t)$ is the temperature difference from the base
321 temperature T_0, and $T = T_0 + T_d$. W_c denotes the deformation energy of per unit volume in the
322 current configuration, and its incompressible viscoelastic expression is assumed as $W_c =$
323 $\frac{1}{2}\int_{-\infty}^{t} G(t-\zeta) \cdot \{\mathrm{d}[\mathrm{tr}(\mathbf{F}_a \cdot \mathbf{F}_a^{\mathrm{T}}) - 3]/\, \mathrm{d}\zeta\}\mathrm{d}\zeta$, where $G(t)$ is the relaxation function. $\kappa(t)$ is
324 another appropriate relaxation function form of the mechanical property. In the expansion, the
325 coupling of viscoelastic deformation and temperature is ignored. The integration functions are
326 continuous for $t > 0$ and are assumed to vanish identically for $t \leq 0$. Substituting Eq. (23)
327 into (22) and doing the indicated differentiation with respect to t, one obtains

328
$$\left(-\mathbf{A}_0 - \frac{\partial W_c}{\partial \mathbf{F}_a} + \sigma \cdot \mathbf{F}_a^{-\mathrm{T}}\right) \cdot \dot{\mathbf{F}}_a + \left(\mathbf{F}_a^{\mathrm{T}} \cdot \sigma \cdot \mathbf{F}_a^{-\mathrm{T}} \cdot \mathbf{F}_g^{-\mathrm{T}} + \mathbf{b}_g \cdot \mathbf{F}_g^{-\mathrm{T}}\right) : \dot{\mathbf{F}}_g + \left[\beta_0 + \int_{-\infty}^{t} \kappa(t-\zeta, 0) \frac{\partial T_d}{\partial \zeta} \mathrm{d}\zeta - \rho s\right] \dot{T} + \left[-\int_{-\infty}^{t} \frac{\partial}{\partial t} \mathbf{A}(t-\zeta) : \frac{\partial \mathbf{F}_a}{\partial \zeta} \mathrm{d}\zeta + \int_{-\infty}^{t} \frac{\partial}{\partial t} \beta(t-\zeta) \frac{\partial T_d}{\partial \zeta} \mathrm{d}\zeta + \rho \dot{d} + -\frac{1}{T} \mathbf{q} \cdot \mathrm{grad}(T)\right] \geq 0. \quad (24)$$

329 In the derivation, the symmetry of the stress and deformation gradient tensor is used. $\mathbf{A}_0 =$
330 $\mathbf{A}|_{t=0}$ is the initial stress and it should be zero in this study. $\beta_0 = \beta|_{t=0}$ is the initial entropy. $\dot{d}$
331 denotes the rate of energy dissipation. Let W as the deformation energy of per unit volume in
332 the virtual configuration, so $W = J_a W_c$. This inequality should be valid for any $\dot{\mathbf{F}}_a$ and $\dot{T}$, that
333 is,

334
$$\sigma = J_a^{-1} \frac{\partial W}{\partial \mathbf{F}_a} \cdot \mathbf{F}_a^{\mathrm{T}}, \quad (25)$$

335
$$\rho s = \beta_0 + \kappa * \mathrm{d}T_d, \quad (26)$$

where $*$ denotes the Stieltjes convolution symbol, $\int_{-\infty}^{t} \phi \frac{\mathrm{d}\varphi}{\mathrm{d}\zeta}\mathrm{d}\zeta = \phi * \mathrm{d}\varphi$. Also, the following inequality can be obtained

$$\left(\mathbf{F}_a^{\mathrm{T}} \cdot \sigma \cdot \mathbf{F}_a^{-\mathrm{T}} \cdot \mathbf{F}_g^{-\mathrm{T}} + \mathbf{b}_g \cdot \mathbf{F}_g^{-\mathrm{T}}\right) : \dot{\mathbf{F}}_g = \left(\mathbf{F}_a^{\mathrm{T}} \cdot \sigma \cdot \mathbf{F}_a^{-\mathrm{T}} + \mathbf{b}_g\right) : \mathbf{L}_g \geq 0. \tag{27}$$

The fourth term of Eq. (24) can result in the dissipation inequality as in the thermoviscoelasticity (Christensen and Naghdi, 1967) and it will not be repeated here.

For illustration, we assume that $\mathbf{L}_g$ has the form

$$\mathbf{L}_g = \sum_i f_i(c_i - c_{i0}) \left(\mathbf{F}_a^{\mathrm{T}} \cdot \sigma \cdot \mathbf{F}_a^{-\mathrm{T}} + \mathbf{b}_g\right). \tag{28}$$

One possible growth model can be obtained, which is a stress-related and nutrient-limited growth model, that is, the local nutrient concentration and residual stresses determine the tissue growth rate. where c_i is the concentration of the constituent i, $f_i(c_i)$ denotes a positive-definite scalar function describing the chemical kinetics, and c_{i0} is the nutrient threshold, below which the tissue reduced in size or dies due to lack of nutrient availability. $(\sigma + \mathbf{b}_g)$ drives the tissue growth and it acts as the biomechanical driving force.

The inequality of Eq. (27) can be satisfied by Eq. (28). Thus Eq. (28) can be written as

$$\dot{\mathbf{F}}_g \cdot \mathbf{F}_g^{-1} = \sum_i f_i(c_i - c_{i0}) \left(\mathbf{F}_a^{\mathrm{T}} \cdot \sigma \cdot \mathbf{F}_a^{-\mathrm{T}} + \mathbf{b}_g\right), \tag{29}$$

which is the growth evolution law. Notably, the growth governing equations are similar to the elastic equations (Xue et al., 2016; Yin et al., 2019), but the stress distribution is related to the viscoelastic properties of tissues.

2.3. Theoretical solution

Many biological tissues have approximately spherical shapes, e.g., tumors and organoids, thus, the spherical model is often used for biological studies (Goriely, 2017). Additionally, the cells at the core may receive less oxygen and nutrients as the sphere grows larger, which leads to the slowed or arrested growth of the core (Walker et al., 2023a). The differential growth rate can also reflect important biological processes. Differential growth rates between the surface and core of spherical structures can lead to important morphogenetic events during tissue development (Eskandari and Kuhl, 2015). In this study, the symmetric growth, deformation, and instability of a spherical shell–core structure are considered as an example to illustrate the prominent features of viscoelastic effects. The shell has inner and outer radii R_i, R_o in the initial

configuration and grows into a sphere shell with inner and outer radii r_i, r_o in the current configuration, as shown in Fig. 4. The interface between the core and the shell is perfectly bonded. The spherical coordinates in the current configuration are (r, θ, φ), and the normal bases are $(\mathbf{e}_r, \mathbf{e}_\theta, \mathbf{e}_\varphi)$. The corresponding coordinates in the initial configuration are (R, Θ, Φ). Thus, the deformation gradient tensor is

$$\mathbf{F} = \mathrm{diag}\left(\frac{\partial r}{\partial R}, \frac{r}{R}, \frac{r}{R}\right). \tag{30}$$

Assuming that in the initial stage of growth, the deformation preserves the spherical symmetry, that is,

$$\mathbf{F}_g = \mathrm{diag}(g_r, g_\theta, g_\theta), \tag{31}$$

where the condition $g_r = g_\theta$ corresponds to the isotropic growth, which means the dilation of original sphere. The mechanical deformation part of the deformation gradient is written as,

$$\mathbf{F}_a = \mathrm{diag}(\alpha_r, \alpha_\theta, \alpha_\theta). \tag{32}$$

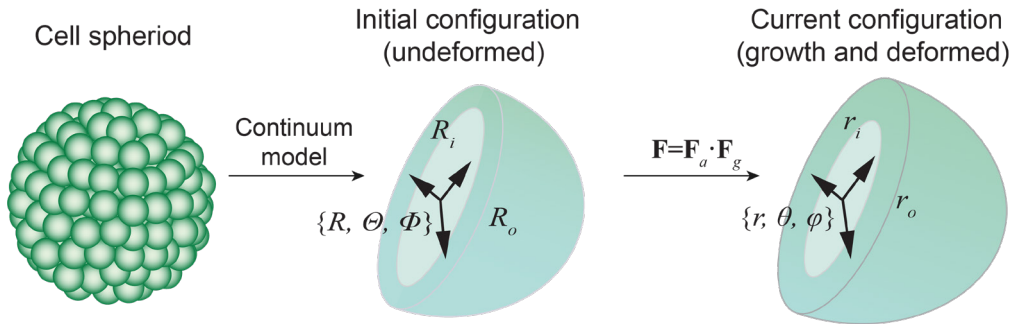

Fig. 4. The spherical shell–core model for a cellular spheroid with differential growth. The shell has the inner and outer radii R_i and R_o in the initial configuration, and it grows to a spherical shell r_i, r_o in the current configuration, respectively. If the core is non-growing, it has $R_i = r_i$. The spherical coordinates (R, Θ, Φ) and (r, θ, φ) are used.

From Eq. (1), one has $\alpha_r = (\partial r / \partial R)/g_r$ and $\alpha_\theta = (r/R)/g_\theta$. The approximation of volume incompressibility requires that $J_a = 1$ and $\alpha_r = \alpha_\theta^{-2}$. Then, the component of $\mathbf{F}$ can be obtained as

$$\frac{\partial r}{\partial R} = \frac{R^2}{r^2} g_r g_\theta^2. \tag{33}$$

By integration, the outer radius is

$$r^3 = r_i^3 + 3\int_{R_i}^{R} g_r\, g_\theta^2 R^2 \mathrm{d}R, \tag{34}$$

and the deformation gradient component can be given as

$$\alpha_\theta = \frac{\left(r_i^3 + 3\int_{R_i}^{R} g_r\, g_\theta^2 R^2 \mathrm{d}R\right)^{\frac{1}{3}}}{g_\theta R}. \tag{35}$$

Taking a time derivative for Eq. (34) and changing the integration variable, the radius evolution equation can be obtained as follows

$$r^2\dot{r} = \int_{R_i}^{R} \dot{g}_r\, g_\theta^2 R^2 \mathrm{d}R + 2\int_{R_i}^{R} \dot{g}_\theta\, g_\theta g_r R^2 \mathrm{d}R = \int_{r_i}^{r} \frac{1}{g_r}\dot{g}_r r^2 \mathrm{d}r + 2\int_{r_i}^{r} \frac{1}{g_\theta}\dot{g}_\theta r^2 \mathrm{d}r. \tag{36}$$

Using Eq. (29), the growth rates in the spherical coordinate system can be obtained as

$$\begin{aligned} \dot{g}_r &= \sum_i f_i(c_i - c_{i0})\left(\sigma_r + b_g\right) g_r, \\ \dot{g}_\theta &= \sum_i f_i(c_i - c_{i0})\left(\sigma_\theta + b_g\right) g_\theta\,. \end{aligned} \tag{37}$$

To focus on the mechanical cues for tissue growth, we consider a spherical shell perfectly bonded on the incompressible non-growing core. The case of isotropic and constant growth ($g_r = g_\theta = g$) is considered (Erlich et al., 2019) as an example. For constant growth, the growth rate is determined by the overall stress state. In this study, the growth equation is simplified as

$$\dot{g} = f_g(c - c_0)\left[\mathrm{tr}(\bar{\sigma}_i) + b_g\right] g, \tag{38}$$

where $\bar{\sigma}_i$ denotes the average of the principle stress components along the radial position, $\mathrm{tr}(\bar{\sigma}_i) = \bar{\sigma}_r + \bar{\sigma}_\theta + \bar{\sigma}_\varphi$. c_0 denotes the critical nutrition density, and the function $f_g(c - c_0)$ describes the effect of nutrient density.

Because of the symmetry, there are only two non-independent stress components in the spherical coordinates, that is, $[\sigma] = \mathrm{diag}(\sigma_r, \sigma_\theta, \sigma_\theta)$. Referring to Eq. (10), the mechanical equilibrium in the spherical coordinate is written as

$$\frac{\partial \sigma_r}{\partial r} + \frac{2}{r}(\sigma_r - \sigma_\theta) = 0. \tag{39}$$

For the incompressible viscoelastic model, W can be written in a form similar to the neo-Hookean material (Khajehsaeid et al., 2014; Narooei and Arman, 2018)

$$W = \frac{1}{2}\int_{-\infty}^{t} G\,(t-\zeta)\frac{\mathrm{d}\left(\alpha_r^2+\alpha_\theta^2+\alpha_\theta^2-3\right)}{\mathrm{d}\zeta}\mathrm{d}\zeta = \frac{1}{2}\int_{-\infty}^{t} G\,(t-\zeta)\frac{\mathrm{d}(\alpha^{-4}+2\alpha^2-3)}{\mathrm{d}\zeta}\mathrm{d}\zeta. \quad (40)$$

where $\alpha = \alpha_\theta$. The relation can be written in the Stieltjes convolution form, that is

$$W = \frac{1}{2}G * \mathrm{d}(\alpha^{-4}+2\alpha^2-3). \quad (41)$$

where $*$ denotes the Stieltjes convolution symbol. The relaxation function $G(t)$ can be approximated by the Prony series as

$$G(t) = G_\infty + \sum_{i=1}^{n} G_i \exp\left(\frac{-t}{\tau_i}\right), \quad (42)$$

where $\tau_i = \xi_i / G_i$ denotes the relaxation time. If we use a simplified viscoelastic model, as shown in Fig. 2c, which is the standard three-parameter model with relaxation time $\tau_g = \xi / G_1$, the relaxation function becomes

$$G(t) = G_\infty + G_1 \exp\left(\frac{-t}{\tau_g}\right). \quad (43)$$

It has the initial modulus $G_0 = G_\infty + G_1$ at time $t = 0$. In the case of isotropic growth ($g_r = g_\theta = g$) and using the stress-free boundary condition $\sigma_r(R_o, t) = 0$, the stress components can be obtained from Eq. (39) and (25) as

$$\sigma_r = \frac{1}{2}G * \mathrm{d}(\alpha^{-4}+4\alpha^{-1}) - \frac{1}{2}G * \mathrm{d}(\alpha_o^{-4}+4\alpha_o^{-1}),$$

$$\sigma_\theta = \sigma_r + \frac{r}{2}\frac{\partial \sigma_r}{\partial r} = \sigma_r + G * \mathrm{d}(\alpha^2+\alpha^{-4}), \quad (44)$$

where

$$\alpha_o = \left(1 - \frac{R_i^3}{R_o^3} + \frac{1}{g^3}\frac{R_i^3}{R_o^3}\right)^{\frac{1}{3}}. \quad (45)$$

The theoretical solution for a growing spherical shell–core structure has been obtained, capturing both its elastic and time-dependent deformation behavior. In the following sections, this model will be applied to specific case studies, focusing on the impact of viscoelasticity on tissue growth and morphological evolution.

3. Growth of a viscoelastic spherical tumor

In growing tumors, the mechanical stress and strain fields, the nutrient and chemical fields, and the growth rates are strongly coupled. The viscoelastic nature of tumors constitutes a pivotal biomechanical attribute that significantly influences tumorigenesis, progression, and metastatic potential (Streitberger et al., 2020; Walker et al., 2023b). Although solid tumors usually evolve irregular shapes as they grow, their initial shapes can be approximated to be spherical. A central necrosis may form in a solid tumor due to the diminished supply of oxygen and nutrients in the core region. As an illustrative case, therefore, the effects of viscoelasticity on tumor growth will be elucidated by using the spherical shell–core model in this section. This model is based on the simplified assumption that the core is incompressible and non-growing, while the outer surface is free to focus on viscoelastic effects.

3.1. Stress field induced by growth

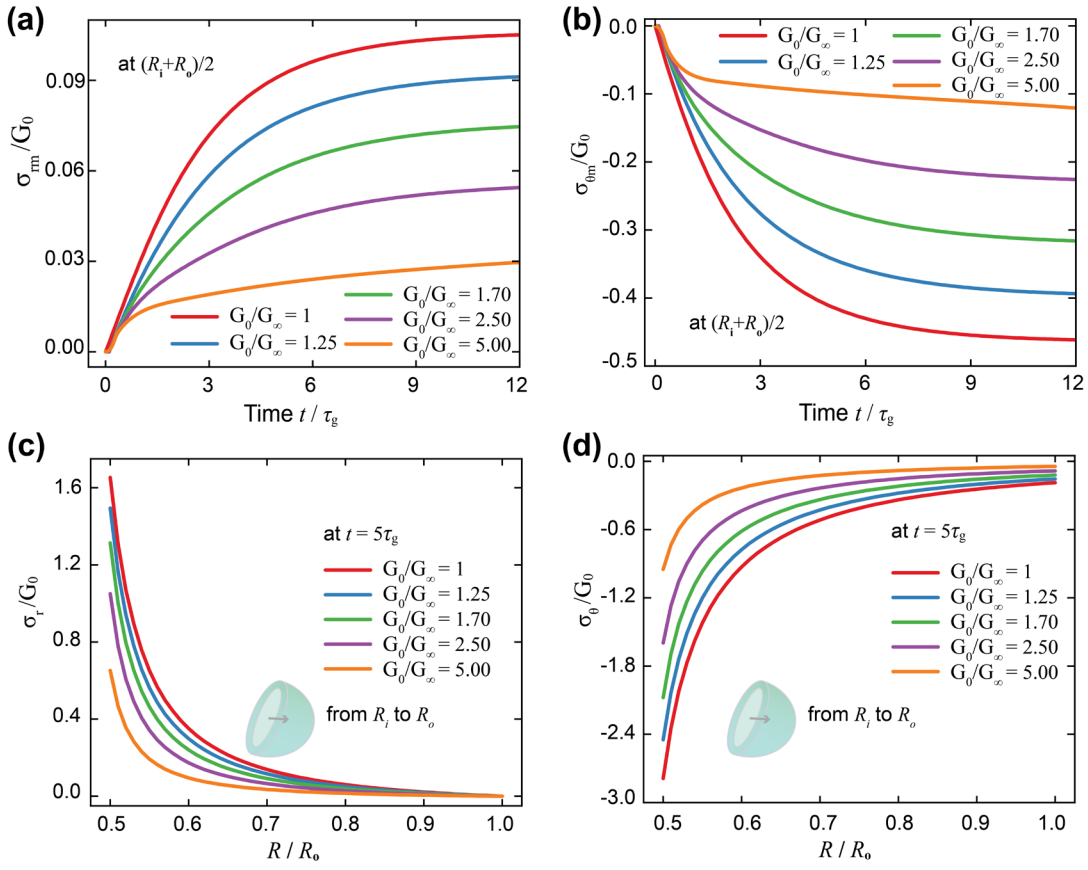

Fig. 5. The stress evolution in a growing spherical shell–core tumor, with geometry $R_i/R_o = 0.5$ and an incompressible non-growing core, that is, the inner surface is fixed and the outer surface is free. A larger G_0/G_∞ indicates more obvious viscoelasticity and stress relaxation, and the difference $G_0 - G_\infty$ denotes the modulus that can be relaxed. All cases have the same initial modulus G_0, and $G_0/G_\infty = 1$ represents the pure elastic case with modulus G_0 and no relaxation. (a, b) The stresses in the med-layer of the spherical

shell change over time for different viscoelastic properties. (c, d) The stresses along the shell thickness at $t = 5\tau_g$ for varying viscoelastic properties.

The differential growth of tissues inherently generates mechanical residual stresses, which evolve with time. The stresses, arising from the continuous cellular proliferation, differentiation, and extracellular matrix remodeling, significantly modulate the biomechanical environment and subsequently influence further growth. The stress accumulation rate is determined by the mechanical properties of the tissue. Fig. 5 illustrates the contrast of residual stresses induced during the processes of elastic and viscoelastic tumor growths. In the elastic tumor (with modulus G_0 and no relaxation, thus is written as $G_0/G_\infty = 1$), stress accumulation increases over time, whereas viscoelasticity facilitates stress relaxation (Fig. 5a-b). Tumors with higher viscoelastic relaxation (larger G_0/G_∞) exhibit slower stress accumulation. As the viscoelastic properties vary, there is a noticeable difference in the stress distribution along the shell thickness (Fig. 5c-d). Stress magnitudes decrease across the spherical shell as the viscoelastic relaxation increases (G_0/G_∞ becomes larger). This indicates that tumors with greater viscoelasticity exhibit more pronounced stress relaxation, thereby reducing the residual stress accumulation more effectively than less viscoelastic or purely elastic tumors. In practice, different tumors present various levels of stress relaxation or viscoelasticity, which may significantly influence their growth and development (Walker et al., 2023b).

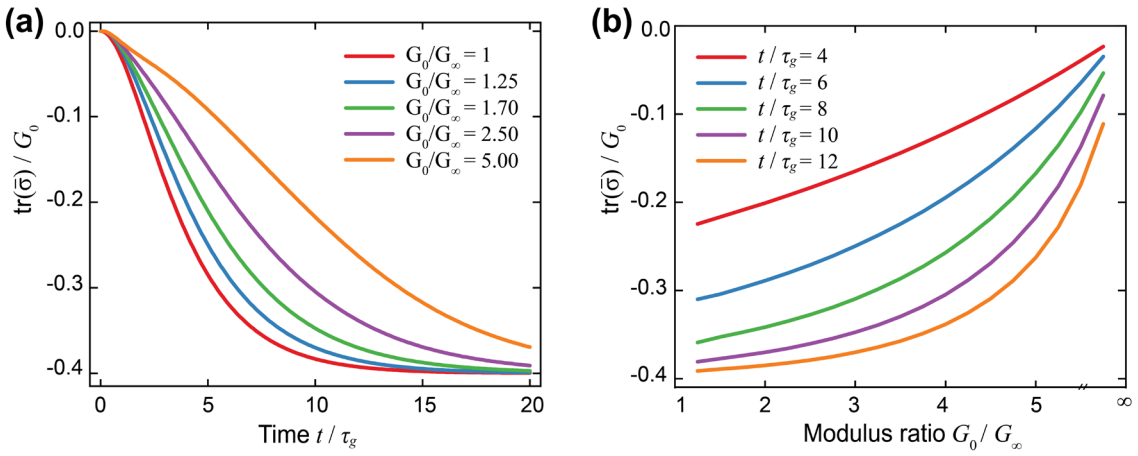

Fig. 6. The sum of the three principal stresses in a growing spherical shell–core tumor, with geometry $R_i/R_o = 0.5$ and an incompressible non-growing core. (a) The variations of the mean principal stresses with time for different viscoelastic properties. (b) The sum of principal stresses versus modulus ratio at different times. All cases have the same initial modulus G_0. A larger G_0/G_∞ corresponds to more obvious viscoelasticity and greater stress relaxation.

The growth equation in Eq. (38) is formulated in terms of the sum of three principal stresses. The accumulation of the total stress is faster in elastic tumors than that in viscoelastic

tumors (Fig. 6). Tumors with lower viscoelasticity (smaller G_0/G_∞) exhibit a higher rate of stress accumulation, as indicated by the curves in Fig. 6a. The relation between the stress and viscoelastic modulus ratio in Fig. 6b demonstrates that the stress accumulation decreases as the viscoelasticity becomes more obvious at any given time. The elastic and viscoelastic properties of tumors determine their capacity for stress management. Elastic tumors maintain higher stress levels over time, whereas viscoelastic tumors experience lower stress levels due to substantial stress relaxation. These findings suggest that viscoelasticity can modify the overall stress level, which may be critical during tumor development. Furthermore, the overall stress state can influence the growth process as described in Eq. (38).

3.2. Growth ratio

Viscoelasticity can significantly influence tumor growth by modulating the stress level, which in turn affects the growth rate. Fig. 7 illustrates the effect of varying viscoelastic properties on the growth ratio and volume, with sufficient nutrient availability. The growth ratio refers to the relative increase in the tumor size. The growth process would stop where the residual stress reaches the maximum value, as described by Eq. (38). For more viscoelastic tumors (larger G_0/G_∞), the growth ratio and the tumor volume exhibit a more pronounced increase with time (Fig. 7a and Fig. 7c). The relations between the growth ratio (or tumor volume) and the modulus ratio can present the effect of viscoelasticity more intuitively (Fig. 7b and Fig. 7d). The growth ratio and volume are greater for more viscoelastic tumors at any given time. The model predicts that the viscoelastic properties are conducive to the growth because of the stress relaxation, which is consistent with the results that residual stresses can inhibit tumor growth (Goriely, 2017; Xue et al., 2016). In addition, the correlation between tumor viscoelasticity and growth rate is in accordance with the reported active particle simulations (Fig. S2), as well as with experimental observations that more fluid glioblastomas grow faster than the more solid meningiomas in the brain (Streitberger et al., 2020).

During the processes of tissue development, wound healing, and lesion formation, the viscoelastic properties of tissues can undergo alteration through cell proliferation, differentiation, and remodeling of ECM (Fig. 2b). This mechanism significantly impacts the subsequent tissue growth. Our model can demonstrate how the changes in the viscoelastic properties affect the growth behavior. For spherical shell–core tumor growth, if the viscoelasticity of a tumor increases as it grows (G_0/G_∞ becomes larger), the growth of the tumor is prolonged and the steady-state volume increases. (Fig. 8a, the green bold curve). In

tumors with higher viscoelasticity, the stresses can be relaxed more effectively, leading to sustained growth compared to those with lower viscoelasticity. Conversely, the tumors with increasing elasticity (G_0/G_∞ becomes smaller) achieve smaller steady-state volumes and cease growing earlier (Fig. 8a, the brown bold curve). These results indicate that the variation in the tissue viscoelasticity during the growth process may establish a feedback loop that further influences tumor progression (Sauer et al., 2023).

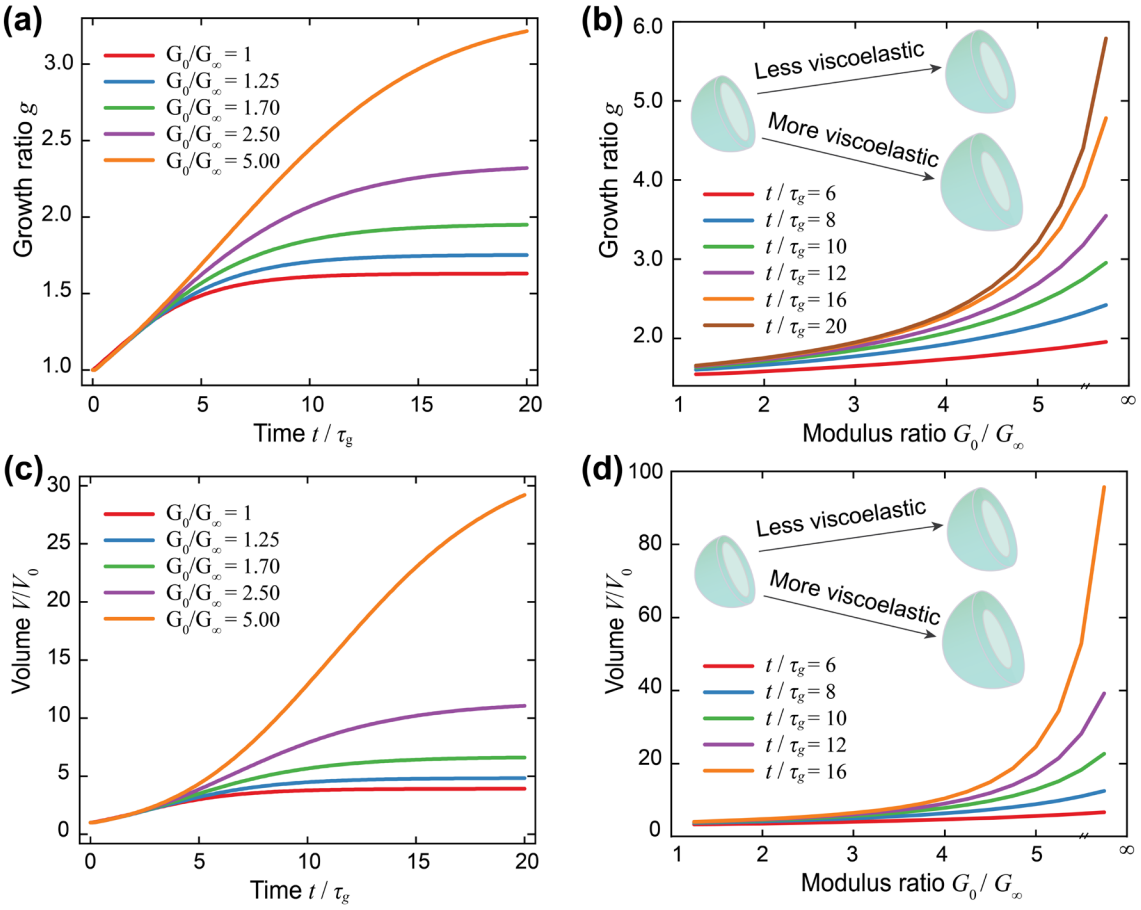

Fig. 7. The growth ratio and volume of a spherical shell–core tumor, with geometry $R_i/R_o = 0.5$ and an incompressible non-growing core. (a) The variations of the growth ratio with time for different viscoelastic properties. (b) The growth ratio versus the modulus ratio at different times. (c) The tumor volume over time for different viscoelastic properties. (d) The tumor volume versus the modulus ratio at different times.

Mechanical factors, including the stresses and moduli, play a significant role in tissue growth. Additionally, tissue growth is influenced by the availability of nutrients (Soleimani et al., 2020; Xue et al., 2016). Eq. (38) describes mechanobiological growth, which is determined by both the stress state and nutrient density. The "nutrient density" includes the availability of essential nutrients, including glucose, amino acids, oxygen, and growth factors. We employ a total nutrient density function to represent these biochemical factors. The interaction between

mechanical stress and nutrient density in growth is illustrated in Fig. 8b. In this discussion, the nutrient is set and will be fully depleted when $V / V_0 = 5$. This setting primarily serves to explore the interplay between mechanical signals and chemical cues during tissue growth. As the nutrients are consumed, the growth rate slows down, but the higher viscoelasticity allows a faster growth rate due to the less accumulation of residual stress. Due to this coupling mechanism, the tumor growth would stop once nutrients are exhausted, even if the critical residual stress has not yet been reached. In addition, the effect of nutrient consumption on growth rate is illustrated by comparison with the sufficient nutrient availability condition (Fig. S3). Consequently, both the residual stress and nutrient density modulate the growth of viscoelastic tumors.

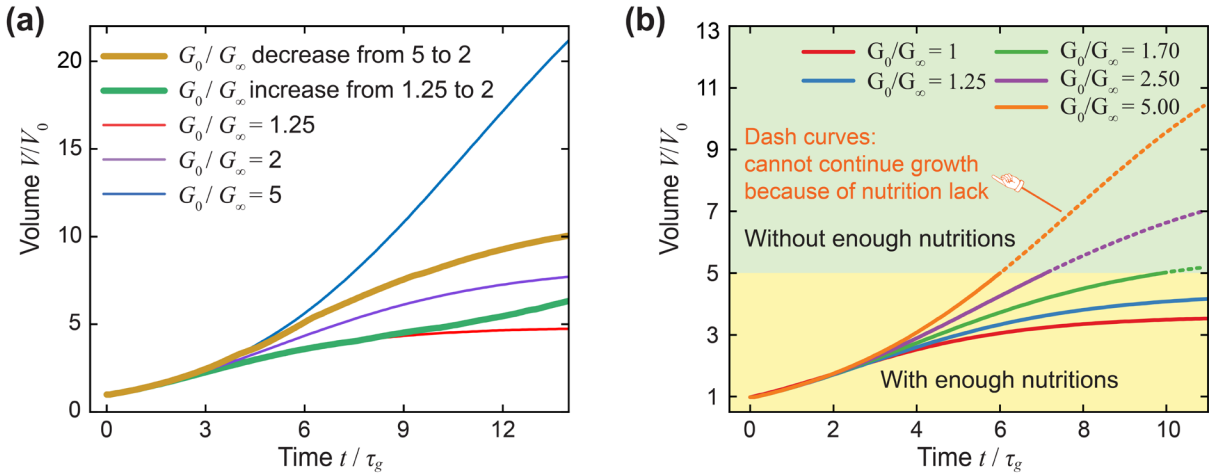

Fig. 8. Influence of viscoelasticity and nutrients on mechanobiological growth. A spherical shell–core structure with geometry $R_i/R_o = 0.5$ and an incompressible non-growing core. (a) Changes in viscoelasticity during growth, resulting in different trends of growth volume. (b) The growth volume of the spherical shell over time, as determined by the residual stress and nutrient availability. In this analysis, the total nutrient supply is constant and the remaining nutrient density is inversely proportional to the growth volume.

3.3. Mechano-chemo-biological mechanisms of viscoelastic growth

Tumor growth is regulated by a complex interplay between mechanical properties and biochemical factors (Sun et al., 2022). Both mechanical stress and viscoelasticity influence cellular behavior through mechano-transduction pathways, and nutrient availability modulates metabolic activities that are essential for cell proliferation and ECM production. The synergistic effects of these factors are crucial for the development and morphogenesis of tissues. The multiscale mechano-chemo-biological mechanism that modulates tissue growth is schematized in Fig. 9. When the cells experience changes in the viscoelastic environment, their

mechano-transduction pathways are activated (Fan et al., 2024). These pathways convert mechanical signals into biological signals, which may regulate gene expression and cell proliferation. Integrins, transmembrane proteins, are responsible for sensing mechanical signals. The mechanical signal activates the Rho/ROCK signaling pathway, which can cause the dynamic evolution of the cytoskeleton. Subsequently, the transcription factor co-activators YAP and transcriptional coactivator with PDZ-binding motif (TAZ) are translocated to the nucleus to induce gene expression (Dupont et al., 2011), thereby promoting cell proliferation and tissue growth. The growth of tissue produces residual stresses, which inhibit further growth. While viscoelastic properties, due to the stress relaxation, can slow down the accumulation of residual stress, thereby facilitating sustained growth. The introduction of these integrated mechano-chemo-biological mechanisms deepens our understanding of tissue growth at multiple length scales, from the molecular, cellular to the tissue scale. This may inspire strategies to adjust various physiological factors for specific therapeutic techniques, which may also be valuable in the fields of tissue engineering and regenerative medicine.

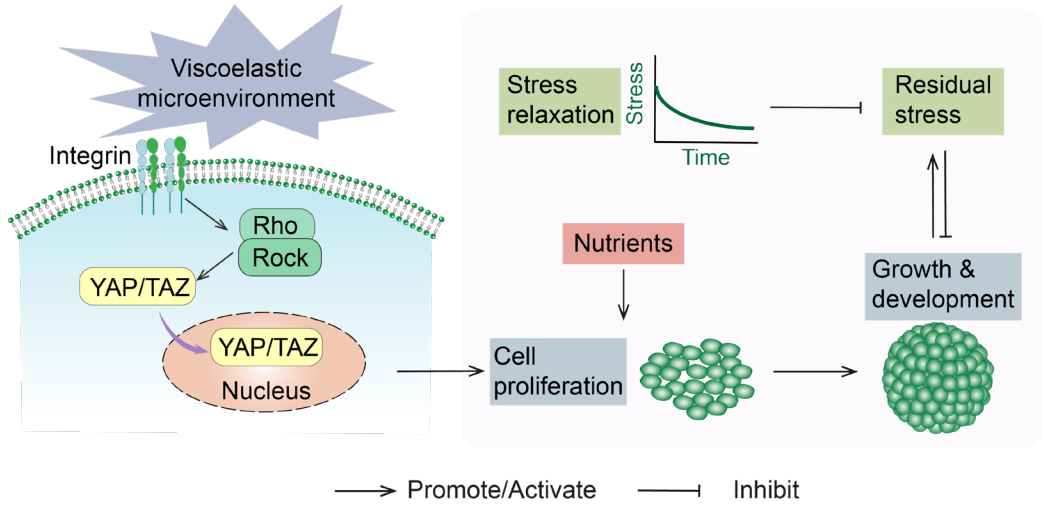

Fig. 9. Multiscale mechano-chemo-biological mechanisms of viscoelastic tissue growth. Integrins sense viscoelasticity, and then influence cell proliferation, which is also affected by nutrient availability. The growth produces residual stresses that inhibit further growth, but the stress will be partly relaxed due to viscoelasticity.

4. Morphological evolution of a growing viscoelastic organoid

Morphogenesis is a key issue in the development of tissues and organs (Yu and Li, 2024). Residual stresses accumulate during tissue growth, and mechanobiological instability may occur when a tissue experiences compressive stresses that exceed a certain threshold, leading to the formation of various surface patterns. On the basis of the above-formulated theory, we

now investigate how viscoelasticity regulates surface instability and the postbuckling morphological evolution of soft tissues.

For illustration, we employ a growing viscoelastic spherical organoid model to elucidate the instabilities arising from tissue growth, with particular attention to the effects of viscoelasticity. For simplicity, the core of the organoid is assumed to be incompressible and non-growing, reflecting the nutrient and oxygen gradients established due to diffusion limitations in the central regions. The peripheral region, conversely, exhibits an enhanced rate of cell proliferation and tissue expansion (Karzbrun et al., 2018). This peripheral growth significantly contributes to the surface tension, potentially leading to buckling at the periphery (Riccobelli and Bevilacqua, 2020). The buckling and postbuckling behaviors are simulated using the finite element method (Abaqus). In the simulation, the four-node axisymmetric elements (CAX4R) are used to discretize the axisymmetric spherical shell–core structure. In the calculations, the mechanical deformation tensor $\mathbf{F}_a$ can be obtained, and then the stresses are determined from $\mathbf{F}_a$ and the viscoelastic modulus of Eq. (43). Finally, the growth state variable is calculated according to Eq. (38), and updated with $g|_{t+\Delta t} = g|_t + \dot{g}|_t \Delta t$.

4.1. Organoids with various viscoelastic properties

We now examine the effects of viscoelastic relaxation on the surface instability of a homogeneous spherical organoid during growth. Fig. 10a shows that, for the same long-term modulus G_∞, viscoelastic growth enters the buckling instability more quickly than purely elastic growth, which is consistent with experimental observations (Elosegui-Artola et al., 2022). It should be noted that the elastic case studied in this section corresponds to the long-term modulus G_∞, and the viscoelastic cases have the same long-term modulus. The morphological evolution of spherical organoids varies with different relaxation times. The occurrence of buckling and the corresponding buckling mode depend on the viscoelastic relaxation rate, even if the modulus ratio remains constant ($G_0/G_\infty = 4$, Fig. 10a). In the case of slow relaxation, residual stresses accumulate rapidly over time, leading to earlier buckling and larger deformation. For medium relaxation, buckling occurs at a moderate growth stage, with a higher buckling mode compared to the case of slow relaxation. The buckling of the fast relaxation case occurs much later, and the patterns resemble those of the elastic case (with the long-term modulus G_∞), as the fast relaxation allows the residual stresses to dissipate quickly, making the relaxation modulus G_1 almost irrelevant. The phase diagram (Fig. 10b) indicates that the relaxation rate determines the critical growth ratio (the maximum growth ratio before

buckling, which is extracted as the mean growth ratio of the last pre-buckling simulation step and the subsequent buckling step.) and the different buckling modes. Organoids with a slower relaxation rate buckle at lower growth ratios because of their faster stress accumulation. This relation highlights the importance of viscoelastic relaxation in determining the stability of growing organoids. Fig. 10c compares the results of our model with previous research, showing that viscoelasticity is associated with a more expeditious morphological evolution, i.e., a faster reduction in circularity compared to elasticity. Circularity, together with morphology and buckling mode, characterizes the morphological evolution process. For the reference results, the circularity is not equal to one because the initial state of their growing spherical tissue is not a perfect sphere. Besides, the thickness ratio and the modulus ratio between the spherical shell and core materials also affect the buckling behavior, which has been discussed in previous literatures (Holland et al., 2017; Huang et al., 2023; Li et al., 2011). This aspect will not be explored in the present study, which instead concentrates on the effect of viscoelasticity.

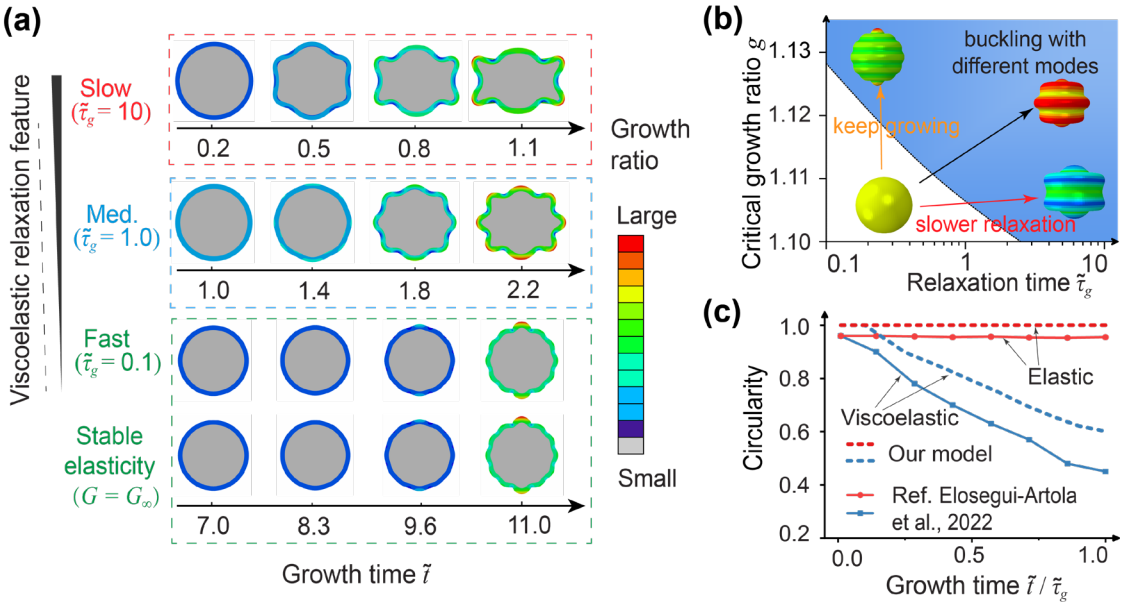

Fig. 10. Instability of the homogeneous viscoelastic spherical shell–core organoids, with $G_0/G_\infty = 4$, geometry $R_i/R_o = 0.9$, and an incompressible non-growing core whose modulus is G_{core}, and $G_\infty/G_{\text{core}} = 3$. (a) The morphology changes of spherical shell–core profile over time, with different relaxation times resulting in different buckling modes. (b) Phase diagram of the critical buckling growth ratio versus relaxation time, with the same long-term modulus G_∞. (c) Comparison with the results in other studies, and our results are calculated with viscoelastic parameters $\tilde{\tau}_g = 5$, $G_0/G_\infty = 4$. The circularity in our results is calculated by $4\pi(S_{\text{area}}) \,/\, (l_{\text{circumference}})^2$, where S_{area} is the area of the middle section, and $l_{\text{circumference}}$ is its circumference. The reference results are from (Elosegui-Artola et al., 2022), and the growth time is normalized. The relaxation time $\tilde{\tau}_g$ and growth time $\tilde{t}$ are made dimensionless by the characteristic growth time $1 \,/\, (f_g^0 G_\infty)$ and the same below, where f_g^0 denotes the initial nutrient effect as in Eq. (38).

The viscoelastic properties of organoids can exert an influence on their morphological evolution after buckling. Simulation results (Fig. 11) show the impact of viscoelastic properties (the relaxation modulus ratio and relaxation time) on the morphology of a growing spherical organoid. Fig. 11a illustrates the morphology of the middle section of the spherical shell–core after buckling, revealing that slower relaxation times lead to more pronounced deformation compared to faster relaxation times. In the slower relaxation time cases, different modulus ratios can lead to different buckling patterns and modes. When the relaxation time is very fast, the initial modulus G_0 will quickly relax to the long-term modulus G_∞, making the increase in the initial modulus (also the modulus ratio G_0/G_∞ in this discussion) has little effect on the overall effective modulus. Circularity, a measure of how closely a shape resembles a perfect circle, is used to measure the rate of morphological evolution. Fig. 11b illustrates the circularity of the middle section of the shell–core for the same evolution time after buckling. The circularity exhibits different trends depending on the relaxation time and modulus. The slow relaxation case corresponds to a steeper curve, indicating a faster rate of evolution. In contrast, the evolution rate caused by the modulus ratio changes is almost negligible in the fast relaxation case. Additionally, the critical growth ratio is also related to the viscoelastic properties (Fig. 11c). A lower critical growth ratio indicates that buckling occurs at a smaller growth volume. This figure indicates that a higher modulus ratio and slower relaxation rate lead to a smaller critical growth ratio, suggesting that only a smaller growth is needed to induce buckling in stiffer tissues.

The relaxation modulus, along with the relaxation time, determines the effective modulus perceived during growth. These properties can influence the buckling behavior of the organoid and the resulting morphological changes. As illustrated in Fig. 12, the results show how viscoelastic properties affect the buckling mode number and critical growth ratio. Different relaxation times and viscoelastic modulus ratios lead to different effective moduli (can be calculated from Eq. (43)). A larger modulus ratio and slower relaxation time lead to fewer mode numbers (Fig. 12a) and smaller critical growth ratios (Fig. 12b), because this condition corresponds to a larger effective modulus and slower stress relaxation, which consequently results in a more rapid accumulation of residual stress. Additionally, higher stability (a larger volume before buckling, corresponding to larger critical growth ratios in Fig. 12b) corresponds to more complex buckling patterns (higher mode numbers). Conversely, lower stability (smaller critical growth ratios) is associated with simpler buckling patterns (lower mode numbers). These relations suggest that the buckling behavior and stability of growing organoids

can be regulated by adjusting the viscoelastic modulus ratio and relaxation time. This understanding may help to develop more effective tissue engineering strategies for the design of artificial tissues and the treatment of diseases characterized by abnormal tissue mechanics. It is also possible that the regulation of viscoelasticity may control the growth and morphogenesis of tissue during natural development, but this hypothesis requires further experimental verification.

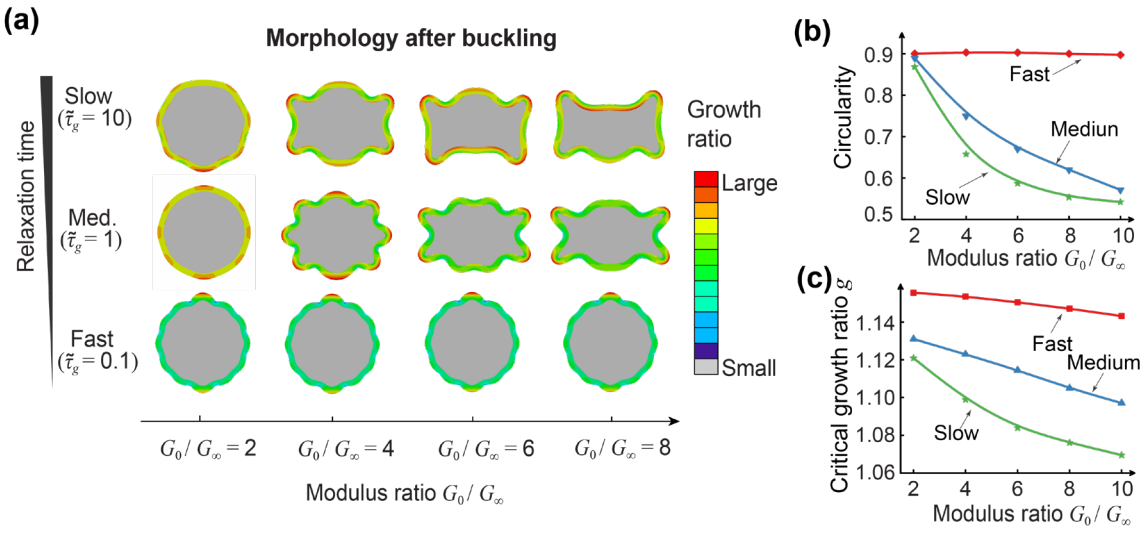

Fig. 11. Morphological evolution of the homogeneous viscoelastic spherical organoids for the same time after buckling (after unit characteristic growth time), with an incompressible non-growing core, the shell geometry $R_i/R_o = 0.9$, and the same long-term modulus G_∞. (a) Morphology of the spherical shell–core profile for different instantaneous moduli G_0 at different relaxation times. A slower relaxation time results in a larger effective modulus. (b) Circularity of the middle section of the spherical shell–core for different relaxation times over the modulus ratio G_0/G_∞, with the same evolution time after buckling. (c) Critical growth ratios (when buckling occurs) over the modulus ratio G_0/G_∞ for different relaxation times. The third configuration in the first row in (a) is symmetrical to the fourth because the rotationally symmetric buckling pattern indicates the same buckling mode for symmetrical geometry. In (b) and (c), the solid line corresponds to a B-spline curve, which is a smooth interpolation of the simulated data points.

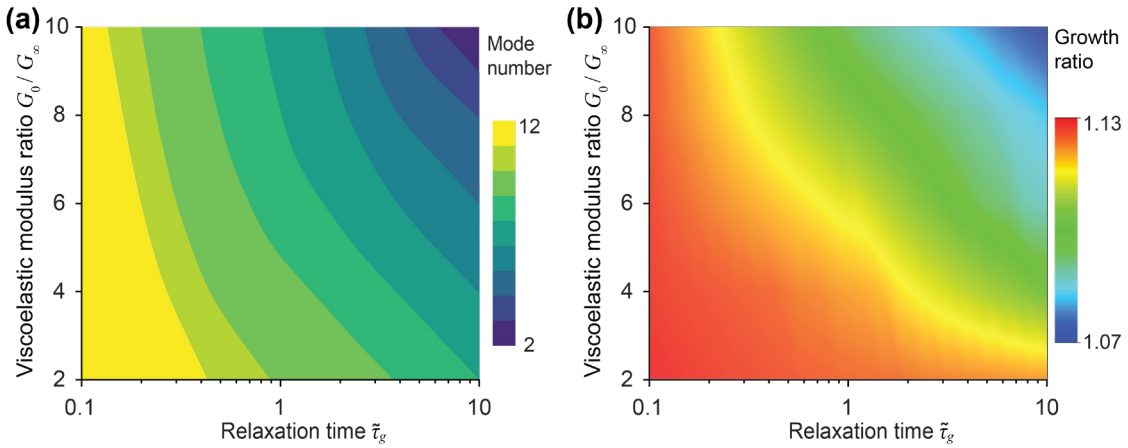

Fig. 12. Phase diagram of the initial buckling mode number and critical growth ratio, with $R_i/R_o = 0.9$, and an incompressible non-growing core. (a) Distribution of mode numbers as a function of viscoelastic modulus and relaxation time. (b) Distribution of critical growth ratios (when buckling occurs) as a function of viscoelastic modulus and relaxation time.

4.2. Viscoelasticity changes during development

During the process of growth, development, and pathological changes, tissues frequently undergo changes in their material properties. Changes in viscoelasticity often play a significant role and can serve as important physiological and pathological indicators (Cox, 2021; Fan et al., 2024; Hiscox et al., 2021). This discussion explores the impact of the transition between fast and slow relaxation times on morphology evolution. Fig. 13 displays how changes in relaxation time influence the morphological evolution of a growing organoid spheroid. The morphology of the spherical shell evolves as the relaxation time changes from fast to slow (Fig. 13a) or slow to fast (Fig. 13c). As the relaxation slows down from a very fast rate, the resulting morphology (the first row of Fig. 13a) differs significantly from the cases with constant relaxation time (the second row of Fig. 13a). The evolution process is accelerated when the relaxation time is slowed, as evidenced by the change of the circularity trends (Fig. 13b). The rate of change in relaxation time (Fast-to-slow-1 vs Fast-to-slow-2 in Fig. 13b) also influences the morphological evolution path and its final state. A faster rate of change results in a faster evolution process. When the relaxation time becomes faster from a slow state, the morphological evolution slows down (the first row of Fig. 13c), and the buckling mode changes during the evolution process. This leads to the nonmonotonic reduction of the circularity curve in Fig. 13d. These differences are driven by variations in the accumulation and dissipation of residual stresses within the tissue. As the viscoelastic properties undergo a transition, the stress accumulation and distribution adjust, leading to different deformation patterns and evolution rates. These results establish a clear link between the dynamic change in viscoelasticity during the development and morphological evolution of organoids. The rate and direction of viscoelasticity changes significantly influence the stability and morphological evolution. This viscoelastic effect on morphological evolution can also be extracted through some experimental observations (Fig. S4). Our findings contribute to a deeper understanding of mechanobiology and offer promising avenues for developing innovative strategies to manipulate tissue growth and address various pathological conditions. For example, adjustable viscoelasticity of biomaterials used in tissue scaffolds may have the potential to enhance their performance in promoting desired tissue growth and integration. In addition, the specific viscoelastic parameters in the theoretical and computational models should be determined by

further series of experimental tests, and then the theoretical and experimental results can be quantitatively compared.

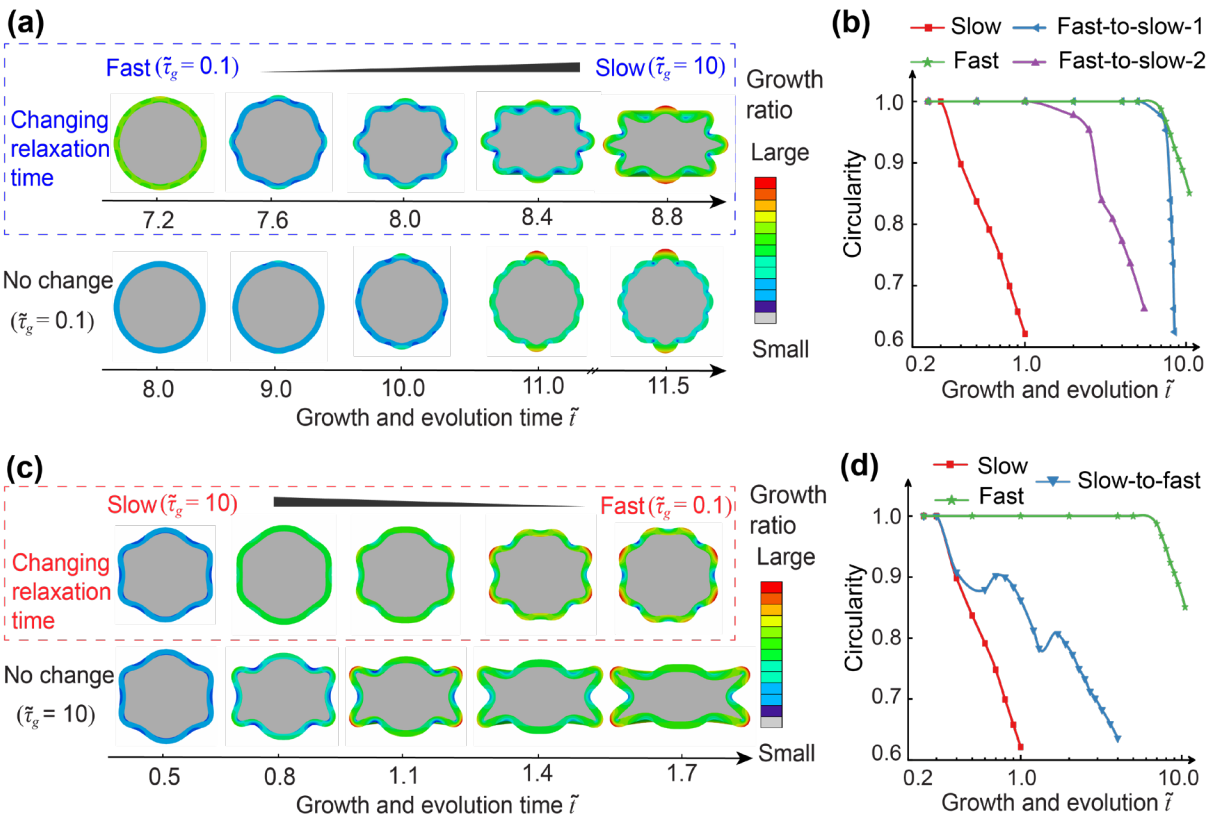

Fig. 13. Morphological evolution of the spherical shell whose viscoelasticity changes during the growth, with $G_0/G_\infty = 4$, $R_i/R_o = 0.9$, and an incompressible non-growing core. (a) Morphology of the middle section over time as the relaxation time changes from fast to slow. (b) The circularity of the middle section for different situations: constant viscoelasticity (Slow and Fast) and relaxation time changing from fast to slow at different rates (Fast-to-slow-1 and Fast-to-slow-2, and Fast-to-slow-2 corresponds to faster changing rate). (c) Morphology of the middle section over time as the relaxation time changes from slow to fast. (d) Circularity of the middle section for different situations: constant viscoelasticity (Slow and Fast) and relaxation time changes from slow to fast (Slow-to-fast).

4.3. Different viscoelastic properties in different regions

Tissues can exhibit different viscoelastic properties across different regions, and these spatial variations can significantly influence their morphological development (Hiscox et al., 2020; Streitberger et al., 2020). Fig. 14a introduces the spatially varying viscoelastic properties within an organoid spheroid and investigates their effects on morphological evolution. The spherical shell model is divided into distinct viscoelastic zones, and each zone exhibits different viscoelastic moduli and relaxation times. In this study, three different cases are considered, where organoids are divided into four, six and ten distinct parts. As observed, the buckling

morphology of the spherical shell shows spatial differences, including the degree of folding and buckling mode number. When the tissue has different viscoelastic properties in different zones, it may grow in various patterns, which might be significant for its function. Our model is capable of simulating how different viscoelastic properties in various regions can modulate tissue folding patterns. This simple model can be further designed to simulate the heterogeneous nature of biological tissues, such as the brain organoid, which exhibit visible differences in folding patterns due to variations in mechanical properties (Fig. 14b). The viscoelastic nature of brain tissue is essential for the formation of cortical folds during development, and it can influence the patterns of gyri and sulci that emerge as the brain grows (Garcia et al., 2018). The spatiotemporal variation in brain viscoelasticity during development is thought to affect neural maturation in different brain regions. This variation contributes to the distinct developmental trajectories of various brain structures, and the brain tissue generally stiffens with maturation, with different regions exhibiting varying degrees of change in their viscoelastic properties (Karzbrun et al., 2018). Our mechanobiological model demonstrates that variations in viscoelastic properties across the tissue can significantly influence its overall morphology. These findings underscore the importance of understanding how regional differences in mechanical properties contribute to the structural and functional diversity of tissues.

The influence of viscoelasticity on morphological evolution can be analyzed in terms of stress accumulation and relaxation dynamics. A region with a slower relaxation rate tends to accumulate residual stress more rapidly because it has less capacity for stress relaxation. This rapid accumulation of stress may not provide sufficient time for the stress to be distributed throughout the tissue, while the adjacent region may have a faster stress relaxation rate. These differences could lead to stress concentrations in certain regions and more abrupt and varied buckling patterns. Further research is needed to establish a clearer relation between specific folding patterns and viscoelastic properties. This could involve collecting additional experimental data or developing more sophisticated computational models that incorporate a wider range of biological factors.

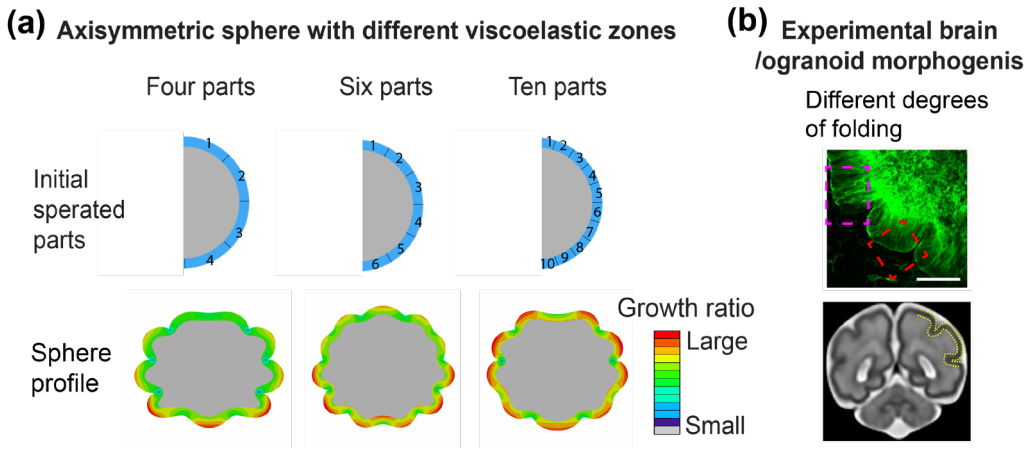

Fig. 14. Morphological evolution of the spherical shell with different viscoelastic parts, with geometry $R_i/R_o = 0.9$, and an incompressible non-growing core. (a) Schematic diagram of spherical shells with different viscoelastic parts and the finite element simulation of the morphological evolution. All parts have the same modulus, i.e., $G_0/G_\infty = 2$, but different relaxation times. The relaxation times for the four parts are $\tilde{\tau}$=0.1, 0.3, 0.4, 0.6, for the six parts are $\tilde{\tau}$=0.1, 0.3, 0.4, 0.6, 0.85, 1.2, and for the ten parts are $\tilde{\tau}$=0.1, 1.5, 0.2, 1.6, 0.1, 1.2, 0.6, 3.0, 0.1, 0.3. (b) Experimental results of the brain or organoid, showing different degrees of folding in different regions, adapted from (Karzbrun et al., 2018) and (Hiscox et al., 2020) .

5. Conclusions

In this paper, we have formulated a mechanobiological model to investigate the influences of viscoelastic properties of soft biological tissues. It provides a theoretical framework for studying the viscoelastic effects on the growth and morphogenesis of soft tissues. Using a spherical shell–core tumor model, it is found that tumors with the same initial modulus but higher viscoelasticity exhibit slower residual stress accumulation, leading to increased growth rates. In addition, nutrient availability also modulates the growth process, with reduced nutrient concentrations leading to decelerated growth over time. The finite element method is used to investigate how viscoelastic properties influence the stability and morphological evolution of growing organoids. The results indicate that for organoids with the same long-term modulus (storage modulus, G_∞), those with higher viscoelasticity enter buckling earlier, in consistency with relevant experimental results (Elosegui-Artola et al., 2022). The relaxation modulus and time determine the buckling mode and subsequent deformation. Furthermore, the variations of viscoelasticity significantly affect growth stability and overall morphology, with changes in viscoelastic properties altering the speed of morphological evolution and potentially shifting the buckling mode. Additionally, organoids with region-specific viscoelastic properties exhibit distinct buckling patterns, providing insight into the diverse morphologies observed during organ development.

By bridging the gap between experimental observations and theoretical modeling, the present theory may help understand the morpho-mechanics of soft tissues (e.g., brains, tumors, and organs-on-a-chip), with potential implications for tissue engineering and disease treatment strategies. Although our model has incorporated some key factors of elasticity and viscoelasticity, the precise functional relation between viscoelastic properties and these factors needs to be elucidated through quantitative series experiments in the future. Besides, there are still many other important mechanisms that may influence the morphological evolution of tissues, such as specific genes or long-term biochemical signaling.

Author contribution

Z. Lin: Writing – review & editing, Writing – original draft, Validation, Software, Methodology, Coding, Investigation, Conceptualization. **W. Huang:** Writing-review & editing, Methodology, Coding, Investigation. **S. Li:** Writing-review & editing, Validation. **M. Wang:** Writing-review & editing, Coding. **J. Bai:** Writing-review & editing, Software. **X. Chen:** Writing-review & editing, Software. **X.-Q. Feng:** Writing-review & editing, Conceptualization, Supervision, Project administration, Funding acquisition.

Declaration of competing interest

The authors declare that they have no known competing financial interests or personal relationships that could have appeared to influence the work reported in this paper.

Acknowledgments

Supports from the National Natural Science Foundation of China (Grant Nos. 12032014 and T2488101) and the Postdoctoral Fellowship Program of CPSF under Grant Number GZC20231309 are acknowledged.

References

Ambrosi, D., Ben Amar, M., Cyron, C.J., DeSimone, A., Goriely, A., Humphrey, J.D., Kuhl, E., 2019. Growth and remodelling of living tissues: perspectives, challenges and opportunities. Journal of the Royal Society Interface 16, 20190233.

Ben Amar, M., Goriely, A., 2005. Growth and instability in elastic tissues. Journal of the Mechanics and Physics of Solids 53, 2284–2319.

Bera, K., Kiepas, A., Godet, I., Li, Y., Mehta, P., Ifemembi, B., Paul, C.D., Sen, A., Serra, S.A., Stoletov, K., Tao, J., Shatkin, G., Lee, S.J., Zhang, Y., Boen, A., Mistriotis, P., Gilkes, D.M., Lewis, J.D., Fan,

C.-M., Feinberg, A.P., Valverde, M.A., Sun, S.X., Konstantopoulos, K., 2022. Extracellular fluid viscosity enhances cell migration and cancer dissemination. Nature 611, 365–373.
Buskohl, P.R., Butcher, J.T., Jenkins, J.T., 2014. The influence of external free energy and homeostasis on growth and shape change. Journal of the Mechanics and Physics of Solids 64, 338–350.
Cambria, E., Coughlin, M.F., Floryan, M.A., Offeddu, G.S., Shelton, S.E., Kamm, R.D., 2024. Linking cell mechanical memory and cancer metastasis. Nat Rev Cancer 24, 216–228.
Chang, Z., Zhang, L., Hang, J.-T., Liu, W., Xu, G.-K., 2023. Viscoelastic Multiscale Mechanical Indexes for Assessing Liver Fibrosis and Treatment Outcomes. Nano Letters 23, 9618–9625.
Chaudhuri, O., Cooper-White, J., Janmey, P.A., Mooney, D.J., Shenoy, V.B., 2020. Effects of extracellular matrix viscoelasticity on cellular behaviour. Nature 584, 535–546.
Chaudhuri, O., Gu, L., Klumpers, D., Darnell, M., Bencherif, S.A., Weaver, J.C., Huebsch, N., Lee, H.-P., Lippens, E., Duda, G.N., Mooney, D.J., 2016. Hydrogels with tunable stress relaxation regulate stem cell fate and activity. Nat. Mater. 15, 326–334.
Christensen, R.M., Naghdi, P.M., 1967. Linear non-isothermal viscoelastic solids. Acta Mechanica 3, 1–12.
Ciarletta, P., Ambrosi, D., Maugin, G.A., 2012. Mass transport in morphogenetic processes: A second gradient theory for volumetric growth and material remodeling. Journal of the Mechanics and Physics of Solids 60, 432–450.
Clément, R., Dehapiot, B., Collinet, C., Lecuit, T., Lenne, P.-F., 2017. Viscoelastic Dissipation Stabilizes Cell Shape Changes during Tissue Morphogenesis. Current biology : CB 27, 3132-3142.e4.
Cox, T.R., 2021. The matrix in cancer. Nat Rev Cancer 21, 217–238.
DiCarlo, A., Quiligotti, S., 2002. Growth and balance. Mechanics Research Communications 29, 449–456.
Ding, K., Lin, Z., Bie, Y., Wei, Y., 2024. The strain gradient viscoelasticity full field solutions for Mode-I and Mode-II crack problems. Engineering Fracture Mechanics 301, 110016.
Dupont, S., Morsut, L., Aragona, M., Enzo, E., Giulitti, S., Cordenonsi, M., Zanconato, F., Le Digabel, J., Forcato, M., Bicciato, S., Elvassore, N., Piccolo, S., 2011. Role of YAP/TAZ in mechanotransduction. Nature 474, 179–183.
Elosegui-Artola, A., Gupta, A., Najibi, A.J., Seo, B.R., Garry, R., Tringides, C.M., Lázaro, I. de, Darnell, M., Gu, W., Zhou, Q., Weitz, D.A., Mahadevan, L., Mooney, D.J., 2022. Matrix viscoelasticity controls spatiotemporal tissue organization. Nature materials 22, 117–127.
Erlich, A., Moulton, D.E., Goriely, A., 2019. Are Homeostatic States Stable? Dynamical Stability in Morphoelasticity. Bull. Math. Biol. 81, 3219–3244.
Eskandari, M., Kuhl, E., 2015. Systems biology and mechanics of growth. Wiley interdisciplinary reviews. Systems biology and medicine 7, 401–412.
Fan, W., Adebowale, K., Váncza, L., Li, Y., Rabbi, M.F., Kunimoto, K., Chen, D., Mozes, G., Chiu, D.K.-C., Li, Y., Tao, J., Wei, Y., Adeniji, N., Brunsing, R.L., Dhanasekaran, R., Singhi, A., Geller, D., Lo, S.H., Hodgson, L., Engleman, E.G., Charville, G.W., Charu, V., Monga, S.P., Kim, T., Wells, R.G., Chaudhuri, O., Török, N.J., 2024. Matrix viscoelasticity promotes liver cancer progression in the pre-cirrhotic liver. Nature, 1–8.
Foroughi, A.H., Valeri, C., Jiang, D., Ning, F., Razavi, M., Razavi, M.J., 2023. Understanding compressive viscoelastic properties of additively manufactured PLA for bone-mimetic scaffold design. Medical Engineering & Physics 114, 103972.
Fung, Y.C., 1990. Biomechanics: Motion, Flow, Stress, and Growth. Springer-Verlag, New York, NY.
Galie, P.A., Georges, P.C., Janmey, P.A., 2022. How do cells stiffen? Biochemical Journal 479, 1825–1842.
Garcia, K.E., Kroenke, C.D., Bayly, P.V., 2018. Mechanics of cortical folding: stress, growth and stability. Philosophical transactions of the Royal Society of London. Series B, Biological sciences 373.
Goriely, A., 2017. The Mathematics and Mechanics of Biological Growth. Springer New York, New York, NY.
Hadzipasic, M., Zhang, S., Huang, Z., Passaro, R., Sten, M.S., Shankar, G.M., Nia, H.T., 2023. Emergence of nanoscale viscoelasticity from single cancer cells to established tumors. Biomaterials 305, 122431.
Hang, J.-T., Xu, G.-K., Gao, H., 2022. Frequency-dependent transition in power-law rheological behavior of living cells. Science advances 8, eabn6093.

Hiscox, L.V., McGarry, M.D.J., Schwarb, H., van Houten, E.E.W., Pohlig, R.T., Roberts, N., Huesmann, G.R., Burzynska, A.Z., Sutton, B.P., Hillman, C.H., Kramer, A.F., Cohen, N.J., Barbey, A.K., Paulsen, K.D., Johnson, C.L., 2020. Standard-space atlas of the viscoelastic properties of the human brain. Human Brain Mapping 41, 5282–5300.
Hiscox, L.V., Schwarb, H., McGarry, M.D.J., Johnson, C.L., 2021. Aging brain mechanics: Progress and promise of magnetic resonance elastography. NeuroImage 232, 117889.
Hobson, E.C., Li, W., Juliar, B.A., Putnam, A.J., Stegemann, J.P., Deng, C.X., 2021. Resonant acoustic rheometry for non-contact characterization of viscoelastic biomaterials. Biomaterials 269, 120676.
Holland, M.A., Li, B., Feng, X.Q., Kuhl, E., 2017. Instabilities of soft films on compliant substrates. Journal of the Mechanics and Physics of Solids 98, 350–365.
Huang, D., Huang, Y., Xiao, Y., Yang, X., Lin, H., Feng, G., Zhu, X., Zhang, X., 2019. Viscoelasticity in natural tissues and engineered scaffolds for tissue reconstruction. Acta biomaterialia 97, 74–92.
Huang, W.-Z., Li, B., Feng, X.-Q., 2023. Mechanobiological tissue instability induced by stress-modulated growth. Soft Matter 19, 708–722.
Huang, W.-Z., Li, B., Feng, X.-Q., 2024. Mechanobiological tortuosity of blood vessels with stress-modulated growth and remodeling. Journal of the Mechanics and Physics of Solids 186, 105605.
Iwashita, M., Kataoka, N., Toida, K., Kosodo, Y., 2014. Systematic profiling of spatiotemporal tissue and cellular stiffness in the developing brain. Development 141, 3793–3798.
Karzbrun, E., Kshirsagar, A., Cohen, S.R., Hanna, J.H., Reiner, O., 2018. Human Brain Organoids on a Chip Reveal the Physics of Folding. Nature physics 14, 515–522.
Katira, P., Bonnecaze, R.T., Zaman, M.H., 2013. Modeling the mechanics of cancer: effect of changes in cellular and extra-cellular mechanical properties. Frontiers in oncology 3, 145.
Khajehsaeid, H., Arghavani, J., Naghdabadi, R., Sohrabpour, S., 2014. A visco-hyperelastic constitutive model for rubber-like materials: A rate-dependent relaxation time scheme. International Journal of Engineering Science 79, 44–58.
Li, B., Cao, Y.-P., Feng, X.-Q., Gao, H., 2011. Surface wrinkling of mucosa induced by volumetric growth: Theory, simulation and experiment. Journal of the Mechanics and Physics of Solids 59, 758–774.
Li, Y., Liu, N., Xie, N., Wei, Z., Liang, X., Xu, F., 2024. Extracellular fluid viscosity: a new physical cue in cell biology. Acta Mechanica Sinica 40, 624056.
Lin, Z., Wei, Y., 2020. A strain gradient linear viscoelasticity theory. International Journal of Solids and Structures 203, 197–209.
Lin, Z., Wei, Y., 2022. The Cross-Scale Strengthening-Softening Behavior of Solids With the Pressurized Cylindrical Cell. Journal of Applied Mechanics 89, 091007.
Lin, Z., Yu, Z., Wei, Y., Wang, Y., 2021. Strain gradient viscoelastic solution and cross-scale hardening-softening behavior for a pressurized thick spherical shell cell. Mechanics of Materials 159, 103902.
Long, Y., Niu, Y., Liang, K., Du, Y., 2021. Mechanical communication in fibrosis progression. Trends in Cell Biology 32, 70–90.
Lyu, C., Kong, W., Liu, Z., Wang, S., Zhao, P., Liang, K., Niu, Y., Yang, W., Xiang, C., Hu, X., Li, X., Du, Y., 2023. Advanced glycation end-products as mediators of the aberrant crosslinking of extracellular matrix in scarred liver tissue. Nat Biomed Eng 7, 1437–1454.
Mao, Y., Wickström, S.A., 2024. Mechanical state transitions in the regulation of tissue form and function. Nat Rev Mol Cell Biol, 1–17.
McGinn, J., Hallou, A., Han, S., Krizic, K., Ulyanchenko, S., Iglesias-Bartolome, R., England, F.J., Verstreken, C., Chalut, K.J., Jensen, K.B., Simons, B.D., Alcolea, M.P., 2021. A biomechanical switch regulates the transition towards homeostasis in oesophageal epithelium. Nat Cell Biol 23, 511–525.
Mierke, C.T., 2022. Viscoelasticity, Like Forces, Plays a Role in Mechanotransduction. Frontiers in cell and developmental biology 10, 789841.
Mongera, A., Pochitaloff, M., Gustafson, H.J., Stooke-Vaughan, G.A., Rowghanian, P., Kim, S., Campàs, O., 2023. Mechanics of the cellular microenvironment as probed by cells in vivo during zebrafish presomitic mesoderm differentiation. Nature materials.

Mongera, A., Rowghanian, P., Gustafson, H.J., Shelton, E., Kealhofer, D.A., Carn, E.K., Serwane, F., Lucio, A.A., Giammona, J., Campàs, O., 2018. A fluid-to-solid jamming transition underlies vertebrate body axis elongation. Nature 561, 401–405.

Morrison, O., Destrade, M., Tripathi, B.B., 2023. An atlas of the heterogeneous viscoelastic brain with local power-law attenuation synthesised using Prony-series. Acta biomaterialia 169, 66–87.

Narooei, K., Arman, M., 2018. Generalization of exponential based hyperelastic to hyper-viscoelastic model for investigation of mechanical behavior of rate dependent materials. Journal of the Mechanical Behavior of Biomedical Materials 79, 104–113.

Panda, S.K., Buist, M.L., 2018. A finite nonlinear hyper-viscoelastic model for soft biological tissues. Journal of Biomechanics 69, 121–128.

Patiño Vargas, M.I., Martinez-Garcia, F.D., Offens, F., Becerra, N.Y., Restrepo, L.M., van der Mei, Henny C., Harmsen, M.C., van Kooten, T.G., Sharma, P.K., 2022. Viscoelastic properties of plasma-agarose hydrogels dictate favorable fibroblast responses for skin tissue engineering applications. Biomaterials Advances 139, 212967.

Pegoraro, A.F., Janmey, P., Weitz, D.A., 2017. Mechanical Properties of the Cytoskeleton and Cells. Cold Spring Harbor perspectives in biology 9, 1–12.

Persson, L.B., Ambati, V.S., Brandman, O., 2020. Cellular control of viscosity counters changes in temperature and energy availability. Cell 183, 1572-1585.e16.

Petridou, N.I., Corominas-Murtra, B., Heisenberg, C.-P., Hannezo, E., 2021. Rigidity percolation uncovers a structural basis for embryonic tissue phase transitions. Cell 184, 1914-1928.e19.

Petridou, N.I., Heisenberg, C.-P., 2019. Tissue rheology in embryonic organization. The EMBO journal 38, e102497.

Rahman, M.M., Feng, Y., Yankeelov, T.E., Oden, J.T., 2017. A fully coupled space–time multiscale modeling framework for predicting tumor growth. Computer Methods in Applied Mechanics and Engineering 320, 261–286.

Rebelo, L.M., Sousa, J.S. de, Mendes Filho, J., Radmacher, M., 2013. Comparison of the viscoelastic properties of cells from different kidney cancer phenotypes measured with atomic force microscopy. Nanotechnology 24, 55102.

Reiter, R., Shahryari, M., Tzschätzsch, H., Haas, M., Bayerl, C., Siegmund, B., Hamm, B., Asbach, P., Braun, J., Sack, I., 2021. Influence of fibrosis progression on the viscous properties of in vivo liver tissue elucidated by shear wave dispersion in multifrequency MR elastography. Journal of the Mechanical Behavior of Biomedical Materials 121, 104645.

Riccobelli, D., Bevilacqua, G., 2020. Surface tension controls the onset of gyrification in brain organoids. Journal of the Mechanics and Physics of Solids 134, 103745.

Rodriguez, E.K., Hoger, A., McCulloch, A.D., 1994. Stress-dependent finite growth in soft elastic tissues. Journal of Biomechanics 27, 455–467.

Rother, J., Nöding, H., Mey, I., Janshoff, A., 2014. Atomic force microscopy-based microrheology reveals significant differences in the viscoelastic response between malign and benign cell lines. Open biology 4, 140046.

Sauer, F., Grosser, S., Shahryari, M., Hayn, A., Guo, J., Braun, J., Briest, S., Wolf, B., Aktas, B., Horn, L.-C., Sack, I., Käs, J.A., 2023. Changes in Tissue Fluidity Predict Tumor Aggressiveness In Vivo. Advanced science (Weinheim, Baden-Wurttemberg, Germany) 10, e2303523.

Soleimani, M., Muthyala, N., Marino, M., Wriggers, P., 2020. A novel stress-induced anisotropic growth model driven by nutrient diffusion: Theory, FEM implementation and applications in bio-mechanical problems. Journal of the Mechanics and Physics of Solids 144, 104097.

Streitberger, K.-J., Lilaj, L., Schrank, F., Braun, J., Hoffmann, K.-T., Reiss-Zimmermann, M., Käs, J.A., Sack, I., 2020. How tissue fluidity influences brain tumor progression. Proceedings of the National Academy of Sciences 117, 128–134.

Sun, S.-Y., Zhang, H., Fang, W., Chen, X., Li, B., Feng, X.-Q., 2022. Bio-chemo-mechanical coupling models of soft biological materials: A review. Advanced in Applied Mechanics 55, 309–392.

Tetley, R.J., Staddon, M.F., Heller, D., Hoppe, A., Banerjee, S., Mao, Y., 2019. Tissue fluidity promotes epithelial wound healing. Nat. Phys. 15, 1195–1203.

Thompson, A.J., Pillai, E.K., Dimov, I.B., Foster, S.K., Holt, C.E., Franze, K., 2019. Rapid changes in tissue mechanics regulate cell behaviour in the developing embryonic brain. eLife 8, e39356.
Walker, B.J., Celora, G.L., Goriely, A., Moulton, D.E., Byrne, H.M., 2023a. Minimal Morphoelastic Models of Solid Tumour Spheroids: A Tutorial. Bulletin of mathematical biology 85, 1–35.
Walker, M., Pringle, E.W., Ciccone, G., Oliver-Cervelló, L., Tassieri, M., Gourdon, D., Cantini, M., 2023b. Mind the Viscous Modulus: The Mechanotransductive Response to the Viscous Nature of Isoelastic Matrices Regulates Stem Cell Chondrogenesis. Adv. Healthcare Mater., e2302571.
Wang, H., Liu, Y.-Q., Hang, J.-T., Xu, G.-K., Feng, X.-Q., 2024. Dynamic high-order buckling and spontaneous recovery of active epithelial tissues. Journal of the Mechanics and Physics of Solids 183, 105496.
Wang, Y., Du, Y., Xu, F., 2023. Strain stiffening retards growth instability in residually stressed biological tissues. Journal of the Mechanics and Physics of Solids 178, 105360.
Wu, Z., Yang, Z., Sha, D., Ma, Y., Kim, B.Y.S., Jiang, W., Yuan, Y., Liu, C., 2022. Injectable, viscoelastic hydrogel precisely regulates developmental tissue regeneration. Chemical Engineering Journal 434, 133860.
Xu, F., Huang, Y., Zhao, S., Feng, X.-Q., 2022. Chiral topographic instability in shrinking spheres. Nat Comput Sci 2, 632–640.
Xue, S.-L., Li, B., Feng, X.-Q., Gao, H., 2016. Biochemomechanical poroelastic theory of avascular tumor growth. Journal of the Mechanics and Physics of Solids 94, 409–432.
Xue, S.-L., Yin, S.-F., Li, B., Feng, X.-Q., 2018. Biochemomechanical modeling of vascular collapse in growing tumors. Journal of the Mechanics and Physics of Solids 121, 463–479.
Yin, S., Li, B., Feng, X.-Q., 2022. Three-dimensional chiral morphodynamics of chemomechanical active shells. Proceedings of the National Academy of Sciences 119, e2206159119.
Yin, S.-F., Xue, S.-L., Li, B., Feng, X.-Q., 2019. Bio–chemo–mechanical modeling of growing biological tissues: Finite element method. International Journal of Non-Linear Mechanics 108, 46–54.
Yu, P., Li, B., 2024. Three-dimensional morphogenesis of epithelial tubes. Acta Mechanica Sinica 40, 623297.
Zhang, K., Zhu, M., Thomas, E., Hopyan, S., Sun, Y., 2021. Existing and Potential Applications of Elastography for Measuring the Viscoelasticity of Biological Tissues In Vivo. Front. Phys. 9, 670571.
Zhou, J., Jiang, L., Khayat, R.E., 2018. A micro–macro constitutive model for finite-deformation viscoelasticity of elastomers with nonlinear viscosity. Journal of the Mechanics and Physics of Solids 110, 137–154.

Appendix A. Transport equation

Let ρ_0 and ρ_g denote densities of the tissue in the initial and virtual states, respectively. The element mass in the virtual state is $\mathrm{d}m_g = \rho_g \mathrm{d}V_g$. Because no mass increases between the virtual and current states, the mass relation is

$$\mathrm{d}m_g = \mathrm{d}m, \qquad \rho_g \mathrm{d}V_g = \rho \mathrm{d}V = \rho J \mathrm{d}V_0 = \rho J_a \mathrm{d}V_g \tag{S1}$$

Thus,

$$\rho_g = \rho J_a \tag{S2}$$

where $\mathrm{d}V_0$ and $\mathrm{d}V_g$ denote the initial and virtual volume elements, respectively. It has $\mathrm{d}V = J\mathrm{d}V_0$ and $\mathrm{d}V_g = J_g \mathrm{d}V_0 = J_a^{-1}\mathrm{d}V$. Besides, the mass growth without flux from the boundaries is,

$$\frac{\mathrm{d}}{\mathrm{d}t}(\rho \mathrm{d}V) = \rho \gamma_g \mathrm{d}V \tag{S3}$$

Let A denote a quality per unit current mass. By using $A\rho dV = A\rho J dV_0$, one has

$$\frac{\mathrm{d}}{\mathrm{d}t}(A\rho \mathrm{d}V) = \frac{\mathrm{d}A}{\mathrm{d}t}\rho \mathrm{d}V + A\frac{\mathrm{d}}{\mathrm{d}t}(\rho \mathrm{d}V) = \frac{\mathrm{d}A}{\mathrm{d}t}\rho \mathrm{d}V + A\rho\gamma_g \mathrm{d}V \tag{S4}$$

and its integration gives

$$\frac{\mathrm{d}}{\mathrm{d}t}\int_\Omega A\rho \mathrm{d}V = \int_\Omega \frac{\mathrm{d}(A\rho)}{\mathrm{d}t}\mathrm{d}V + \int_\Omega A\rho \,\mathrm{div}\,\mathbf{v}\,\mathrm{d}V = \int_\Omega \rho \frac{\mathrm{d}A}{\mathrm{d}t}\mathrm{d}V + \int_\Omega \rho\gamma_g A \mathrm{d}V \tag{S5}$$

which is the growth rate related transport equation.

Appendix B. Multiscale viscoelastic model

Viscoelasticity of tissue can be expressed as the effects of several key factors at multiscale. These effects may be simplified and abstracted as a modulus function, i.e., $G = f(D, C, M, A, R)$, where $D, C, M, A,$ and R denote the effect of cell density, cell types, ECM property, adhesion effect, and cytoskeleton evolution, respectively (Fig. S1a). In the following, we illustrate the relations between viscoelastic parameters and the cell-to-tissue phenomena.

Experimental studies have shown that the cell density varies in different regions of zebrafish embryos along the AP axis (Mongera et al., 2023). The modulus and viscosity decrease as the extracellular spaces between cells increase (Fig. S2b). Therefore, we can simply give the relation between cell density and viscoelastic parameter, as

$$G_{D\infty} = \frac{k_1}{D_{\text{density}}}, \qquad \xi_D = \frac{k_2}{D_{\text{density}}}, \tag{S6}$$

where $G_{D\infty}$ and ξ_D are the long-term modulus and viscosity parameter due to the effect of cell density, and k_1 and k_2 are two parameters to be determined.

For the adhesion effect, drawing on the relation between cell-cell tension and tissue viscosity in the previous study (Fig. S1c), we can simply give

$$\xi_A = k_3 \exp(A_{\text{c-adhesion}}) + k_4 \exp(A_{\text{i-adhesion}}), \tag{S7}$$

where ξ_A is the viscosity parameter due to the effect of adhesion, $A_{\text{c-adhesion}}$ and $A_{\text{i-adhesion}}$ correspond to cell-cell adhesion and cell-matrix adhesion, respectively, k_3 and k_4 are parameters to be determined. For the ECM effect, previous studies have shown that the stiffness and viscosity increase with as liver fibrosis (Fan et al., 2024; Lyu et al., 2023; Fig. S1d). Therefore, we try to give the relation

$$\begin{aligned} G_{M\infty} &= k_5 M_{\text{n-fibril}} + k_6 M_{\text{n-crosslinker}}, \\ \xi_M &= k_7 M_{\text{n-fibril}} + k_8 M_{\text{n-crosslinker}}, \end{aligned} \tag{S8}$$

where $G_{M\infty}$ and ξ_M are the long-term modulus and viscosity parameter of ECM, $M_{\text{n-fibril}}$ and $M_{\text{n-crosslinker}}$ correspond to the density of fibrils and crosslinkers, respectively, $k_5 \sim k_8$ are parameters to be determined.

Different types of cells have various stiffness and viscosity. Simply, we can use the homogenization method to obtain the modulus and viscosity in a representative element, as

$$G_{C\infty} = \frac{\sum_{i=1}^{n} G_i V_i}{V}, \qquad \xi_C = \frac{\sum_{i=1}^{n} \xi_i V_i}{V}, \tag{S9}$$

where $G_{C\infty}$ and ξ_C are the long-term modulus and the viscosity parameter that combine different types of cells, G_i, ξ_i and V_i are the long-term modulus, viscosity parameter and volume of the i type cell, V is the total volume of the representative element. The cytoskeleton and cell contractility can influence the viscoelasticity of a cell (Galie et al., 2022; Yin et al., 2022). This effect in captured in G_i and ξ_i, while the quantitative metrics for viscoelastic parameters need further study.

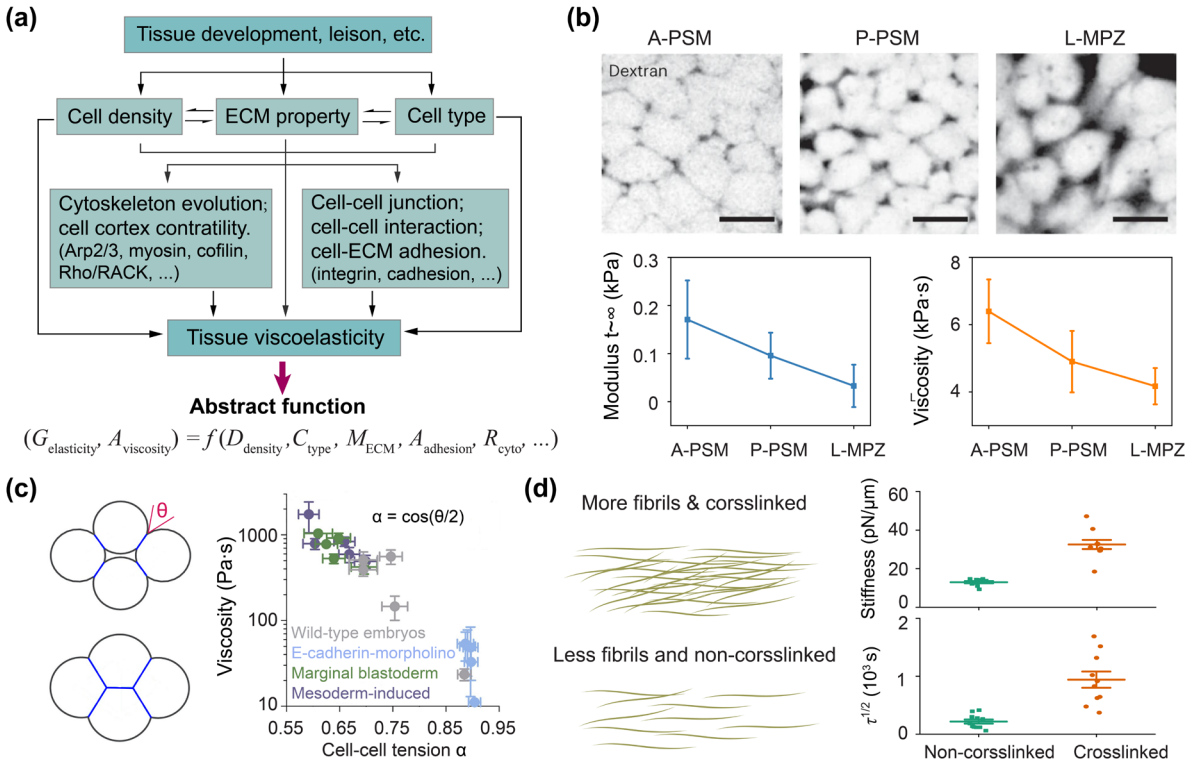

Fig. S1. Multiscale viscoelastic mechanisms. (a) Methodology to correlate macroscopic viscoelasticity with underlying multiscale mechanisms. (b) Viscoelasticity varies with cell density in different parts of zebrafish embryos, where A-PSM: presomitic mesoderm in the AP axis, P-PSM: posterior presomitic mesoderm, MPZ: lateral part of the mesodermal progenitor zone (Mongera et al., 2023). (c) Influence of cell-cell adhesion on tissue viscosity (Petridou et al., 2021). (d) Schematic of ECM fibrils and crosslinking (left) and modulation of crosslinking on collagen matrix (right, Lyu et al., 2023). Longer relaxation time $\tau^{1/2}$ corresponds to larger viscosity.

Eqs. (S6-S9) represent different scale influences on viscoelasticity. To combine these multiscale effects, we may borrow ideas from the cross-scale viscoelasticity theory (Ding et al., 2024; Lin et al., 2021; Lin and Wei, 2022, 2020). We write the total potential energy density as

$$w = \frac{1}{2}(G_D * \mathrm{d}\varepsilon_D * \mathrm{d}\varepsilon_D + G_A * \mathrm{d}\varepsilon_A * \mathrm{d}\varepsilon_A + G_M * \mathrm{d}\varepsilon_M * \mathrm{d}\varepsilon_M + G_C * \mathrm{d}\varepsilon_C * \mathrm{d}\varepsilon_C), \quad \text{(S10)}$$

where $G_{\blacksquare}$ denotes the viscoelastic modulus related to different effects, $\varepsilon_{\blacksquare}$ is the corresponding strain, $*$ is the Stieltjes convolution symbol. The Stieltjes convolution is defined as $\phi * \mathrm{d}\varphi = \int_{-\infty}^{t} \phi(t-\zeta)\dot{\varphi}(\zeta)\mathrm{d}t$. Strains from different scales can be related. If we give an effective strain ε_{e}, the corresponding effective stress can be $\sigma_{\mathrm{e}} = \partial w/\partial \varepsilon_{\mathrm{e}}$. The stress can be written as $\sigma_{\mathrm{e}} = G * \mathrm{d}\varepsilon_{\mathrm{e}}$, where G is the effective modulus, as

$$G = f(D, C, M, A, R, t). \quad \text{(S11)}$$

It should consist of a purely elastic part (long-term modulus G_∞), a viscous part (viscosity ξ), and a related elastic part G_1 at least to characterize the relaxation time together with ξ. To explicitly show the effect of viscoelasticity, we combine these parameters based on the three-parameter viscoelastic model (Fig. 2c). Therefore, the effective modulus can be written as $G(t) = G_\infty + G_1 \exp(-t\ G_1\ /\xi)$. The changes in viscoelastic modulus and relaxation time during tissue development (Section 4, Fig. 10) are related to multiscale mechanisms. For example, the increase in modulus and viscosity may correspond to the process of fibrosis or cell jamming.

However, the influence of multiscale phenomena cannot be completely separated. For example, the difference in cell density in Fig. S1b would involve cell-cell adhesion. The change in ECM property would also influence cell-ECM adhesion. This section only presents a rough equivalent thought and methodology. Further experimental and theoretical studies are needed to capture the complex relation between multiscale mechanisms and viscoelastic parameters.

Appendix C. Viscoelastic effects on tissue growth

Our model predicts that viscoelastic properties facilitate tissue growth by reducing the rate of residual stress accumulation. This is consistent with the stress-induced growth studies, where smaller residual stress is beneficial for growth. Furthermore, we compare our results with the simulation results reported by Elosegui-Artola et al., as shown in Fig. S2. Their study investigates tissue growth in viscoelastic and elastic environments using a four-parameter viscoelastic model, and the observed trends regarding the influence of viscoelasticity on growth rates are consistent with our findings. Besides, different viscoelastic models have been used to characterize the viscoelasticity of tissues, such as the Maxwell model, the three-parameter model, the four-parameter model, and the generalized Maxwell model. In this paper, we use the widely used three-parameter model.

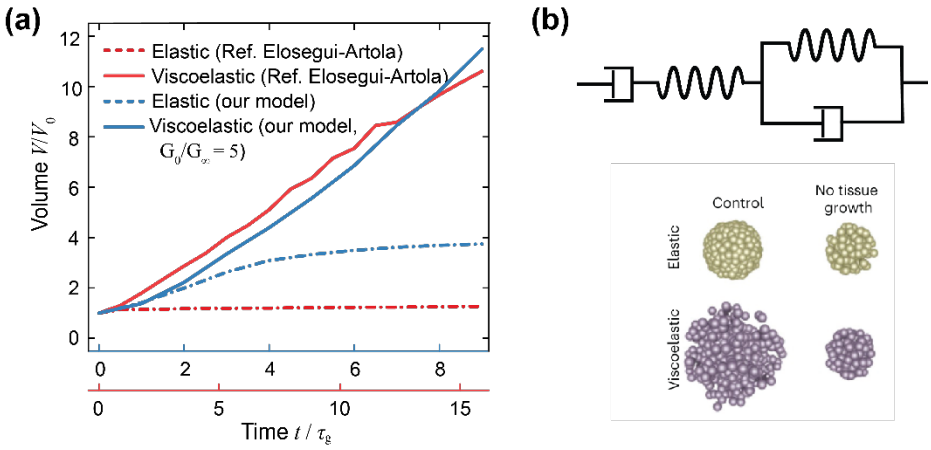

Fig. S2. Comparison between our results and some previous studies on the viscoelastic effects on tissue growth. (a) Comparison between our model and the active particle simulations made by Elosegui-Artola et al. (b) The four-parameter viscoelastic parameter and an active particle model used by Elosegui-Artola et al.

Appendix D. Effects of nutrition consumption

The mechanobiological growth of soft biological tissues is determined by both stress state and nutrient density. Nutrients can include the availability of essential nutrients, including glucose, amino acids, oxygen, and growth factors. We use a total nutrient density function to represent these biochemical factors. The comparison between the sufficient and limited nutrient availability conditions is illustrated in Fig. S3. It shows that limited nutrient availability may significantly slow the growth rate.

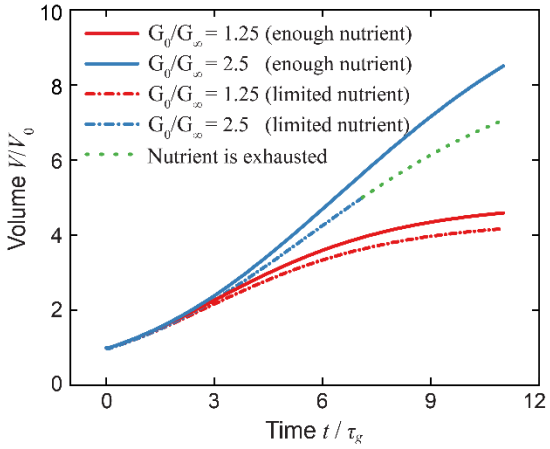

Fig. S3. Effects of nutrient density on tissue growth. The solid curves correspond to the sufficient nutrient availability condition, i.e., nutrient density does not decrease during growth. The dash-dot curves correspond to the limited nutrient availability condition, where the total nutrient supply remains constant, and the nutrient density decreases linearly as the growth volume increases.

Appendix E. Effects of viscoelastic changes on morphological evolution

During tissue development, viscoelasticity can change, which may be be significant for the morphological evolution (Iwashita et al., 2014; Petridou and Heisenberg, 2019; Thompson et al., 2019). Fig. S4 shows the brain folding progress (Fig. S4a) and viscoelasticity during tissue development (Fig. S4b-c). It indicates that the viscoelasticity changes can influence the morphological changes, in qualitative consistency with our simulations, as shown in Fig.13. Studying the effect of relaxation time transitions on morphological evolution would require detailed parameterization in experiments.

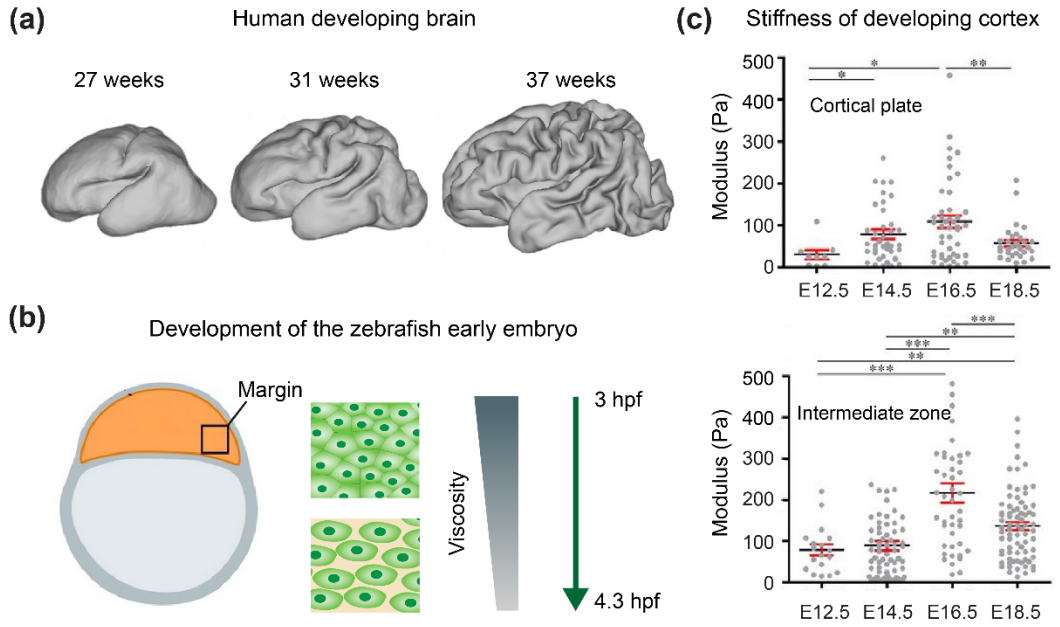

Fig. S4. Changes of viscoelasticity in developing brains and embryos. (a) Cortical folding progress is shown after birth in preterm human (Garcia et al., 2018). (b) Viscosity of zebrafish early embryos from the blastula (3 hpf) to the dome stage (4.3 hpf) (Petridou and Heisenberg, 2019). (c) Stiffness of developing mice cortex, where E12.5, E14.5, E16.5, and E18.5 denote different embryonic stages (Iwashita et al., 2014).